TECHNISCHE UNIVERSITÄT DRESDEN

Faculty of Environmental Sciences

Water Quality Simulation with Particle Tracking Method

Dissertation for awarding the academic degree
Doctor rerum naturalium (Dr. rer. nat.)

Submitted by
M.Eng. Yuanyuan Sun
Date of birth: 09.11.1983
Place of birth: Shandong, China

Supervisor:

Mr. Prof. Dr.-Ing. Olaf Kolditz
Technische Universität Dresden / Helmholtz Zentrum für Umweltforschung - UFZ

Mr. Prof. Dr. Rudolf Liedl
Technische Universität Dresden

Dresden, 07.11.2013

Explanation of the doctoral candidate

This is to certify that this copy is fully congruent with the original copy of the dissertation with the topic:

„Water Quality Simulation with Particle Tracking Method“

……
Place, Date

……
Signature (surname, first name)

Acknowledgments

The first person I would like to express my gratitude is without doubt my supervisor Prof. Dr.-Ing Olaf Kolditz, the head of the Department of Environmental Informatics in the Helmholtz Centre for Environmental Research - UFZ, Leipzig. He offered me the opportunity to carry out my research as a PhD student and instructed me with my work. His wisdom and knowledge inspire me and his optimism and enterprise encourage me. I can't express to him how grateful I am for his help. I also would like to sincerely thank my supervisor Prof. Dr. Rudolf Liedl, head of the Institute for Groundwater Management, Department of Hydrosciences, TU Dresden. His advices help a lot with my work. I wish to give my special thanks to Dr. Wenqing Wang for helping me with the implementation of my model and solving programming problems.

I would like to take this opportunity to give my sincere thanks to all my colleagues at the Department of Environmental Informatics and the OpenGeoSys Community. I want to thank Dr. Chan-Hee Park for establishing the structure of the RWPT model. Great thanks go to Dr. Haibing Shao and Dr. Norihiro Watanabe for their inspirations and discussions. I would like to thank Dr. Thomas Kalbacher for being my mentor and encouraging me a lot. Many thanks to Dmitri Naumov for the preparation of pore scale mesh files. I want to thank the first floor group - Dr. Thomas Fischer, Dr. Karsten Rink, Dr. Lars Bilke for their help with meshing problems. I would like to give my warm and sincere thanks to Dr. Hua Shao and Herbert Kunz from German Federal Institute for Geosciences and Natural Resources (BGR) for their kind help. And also many thanks to Sindy Rosenkranz-Bleiholder, Nora Eigenwill and Victor Weiler for their help with office management.

My work was kindly supported by Helmholtz Association - China Scholarship Commission program and Helmholtz Impulse and Networking Fund through Helmholtz Interdisciplinary Graduate School for Environmental Research (HIGRADE). I would like to express my gratitude to Dr. Vera Bissinger and Barbara Timmel from HIGRADE for providing convenience for my studying and staying in UFZ.

I am grateful for the love and support from my beloved parents and my boyfriend. They give me the strength to carry on and a reason to live a better life. I also want to thank all my relatives for their kind care for me. I would like to thank all my friends for their company and encouragement. For my dearest friends, it is needless to say how much our friendship means to me. I sincerely thank all the people who have helped me.

And I would like to thank the city Leipzig for giving me happy memories that I will cherish forever.

Yuanyuan Sun
Leipzig
February 2013

Abstract

In the numerical simulation of fluid flow and solute transport in porous media, finite element method (FEM) has long been utilized and has been proven to be efficient. In this work, an alternative approach called random walk particle tracking (RWPT) method is proposed. In this method, a finite number of particles represent the distribution of a solute mass. Each particle carries a certain fraction of the total mass and moves in the porous media according to the velocity field.

The proposed RWPT model is established on a scientific software platform OpenGeoSys (OGS), which is an open source initiative for numerical simulation of thermo-hydro-mechanical-chemical (THMC) processes in porous media. The flow equation is solved using finite element method in OGS. The obtained hydraulic heads are numerically differentiated to obtain the velocity field. The particle tracking method does not solve the transport equation directly but deals with it in a physically stochastic manner by using the velocity field. Parallel computing concept is included in the model implementation to promote computational efficiency.

Several benchmarks are developed for the particle tracking method in OGS to simulate solute transport in porous media and pore space. The simulation results are compared to analytical solutions and other numerical methods to test the presented method. The particle tracking method can accommodate Darcy flow as it is the main consideration in groundwater flow. Furthermore, other flow processes such as Forchheimer flow or Richards flow can be combined with as well. Two applications indicate the capability of the method to handle theoretical real-world problems. This method can be applied as a tool to elicit and discern the detailed structure of evolving contaminant plumes.

Nomenclature

Table 1: Latin symbols

Symbol	Meaning	Unit
A	Area	m^2
C	Solute concentration	kg/m^3
D	Hydrodynamic dispersion tensor	m^2/s
D_d	Molecular diffusion tensor	m^2/s
$\mathbf{f}$	Body forces	N/m^3
g	Gravitational acceleration	m/s^2
h	Piezometric head (hydraulic head)	m
k	Intrinsic permeability	m^2
k_r	Relative hydraulic conductivity	-
K	Hydraulic conductivity tensor	m/s
l	Length	m
M	Mass	kg
n	Porosity	-
N	Number of particles	-
p_c	Capillary pressure	Pa
P	Pressure	Pa
P_V	Pore volume	-
q	Volumetric flux	m/s
Q	Volumetric flow rate	m^3/s

Table 1 – Continued from previous page

Symbol	Meaning	Unit
R	Retardation factor	-
S	Saturation	-
S_e	Effective water saturation	-
S_s	Volumetric specific storage	$1/m$
t	Time	s
x, y, z	Cartesian coordinates	m
$\mathbf{v}$	Velocity vector	m/s
V	Volume	m^3
z	Elevation head	m
Z	Random number	-

Table 2: Greek and math symbols

Symbol	Meaning	Unit
α_T	Transverse dynamic dispersivity	m
α_L	Longitudinal dynamic dispersivity	m
β	Forchheimer coefficient	$1/m$
δ_{ij}	Kronecker symbol	-
θ	Volumetric water content (moisture content)	-
λ	Filtration coefficient	m^{-1}
μ	Dynamic viscosity	$Pa \cdot s$
ρ	Material density	kg/m^3
ψ	Pressure head	m
Ω	Control volume, representative elementary volume (REV)	-
∇	Gradient operator	
$\nabla\cdot$	Divergence operator	
∇^2	Vector Laplacian	
∂	Partial differential	

Contents

List of Tables

List of Figures

Chapter 1

Introduction

1.1 State of the art

1.1.1 Background

In the simulation of solute transport in porous media, the advection-dispersion equation (Bear, 1979) is usually adopted as governing equation, which can be solved by standard finite difference method and finite element method. These methods may suffer from the numerical dispersion or artificial oscillations unless a high grid resolution and small time steps are applied. An alternative is the particle tracking method which does not have the Peclet constraint, thus is applicable especially for the advection-dominated problems.

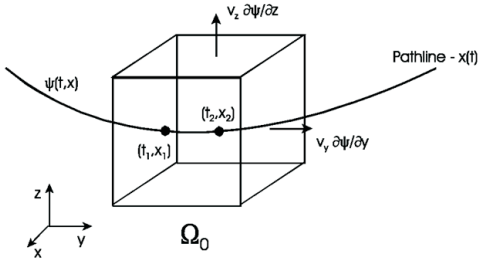

Figure 1.1: Euler-Lagrangian conception (Kolditz, 2002)

The basic idea of particle tracking is that a finite number of particles represent the distribution of a solute mass. Each particle carries a certain concentration or a certain

fraction of the total mass and moves in the porous media according to the velocity field and dispersive process. The concentration distribution of the system is converted from particle clouds by spatial discretization and counting of particles in the cell. The particle tracking method does not solve the transport equation directly; instead, it uses the flow velocities obtained from the solution of the flow equation to advect the particles, and adds some additional displacement to simulate dispersion.

One of the earliest numerical techniques within particle tracking concept is the Method of Characteristics (MOC). Konikow and Bredehoeft (1978) developed the code MOC which became very popular at that time. The computer-generated particle is considered to be representative of some control volume and moves along pathlines in the velocity field. The processes of dispersion, decay, and retardation can be considered separately in MOC. There are some limitations of this method, for example, the grid Courant constraint is necessary to control particle migration to no more than one cell length per time step; particles should be distributed throughout the whole calculating domain even if there is no concentration in some area.

Another numerical technique named Random Walk Particle Tracking (RWPT) was introduced by Prickett et al. (1981). The random walk method was from statistical physics which was original used in the analysis of dispersion and diffusion processes in porous media (De Josselin de Jong, 1958; Scheidegger, 1954). The RWPT method was developed for the simulation of solute transport in aquifers, including the effects of convection, dispersion, and chemical reactions. In this method, each particle represents a fixed mass, and moves through the calculating domain with two types of motion: one with the mean flow, and one with the random dispersion. Enough particles are included to describe the distribution of the solute concentration.

1.1.2 Advantages and limitations of RWPT

The RWPT method has good computational efficiency compared to MOC. Particles are needed only in places that the concentration distribution is of interest, rather than everywhere of the calculation domain.

The RWPT method is free of numerical dispersion in advection-dominated problems

because the particle's jump obeys the exact scaling with the square root of time characteristic for normal diffusion.

Since no particle is lost nor destroyed during the simulation, the method is inherently mass conservative.

Another advantage is that the RWPT method can be implanted over different type of flow model.

One of the limitations of this method is that the computed concentrations have random fluctuations. That is because of the statistical nature of this method. The relative size of these fluctuations can be diminished by increasing the number of particles.

Another limitation is that RWPT may be computational expensive because a large number of particles are needed to get the smooth distribution of concentration. On the other hand, the particle number must be restricted, because each particle is independent and needs memory to record the information of its moving history.

1.1.3 Applications

RWPT method has been used for modeling solute transport in aquifers(Prickett et al., 1981), complex, high-resolution transport problems(Tompson and Gelhar, 1990; Tompson et al., 1998), advective-dispersive transport in composite media(LaBolle et al., 2000), fractional-order multiscaling anomalous diffusion(Zhang et al., 2006), non-Fickian transport(Srinivasan et al., 2010).

There are other concepts of particle tracking methods, for instance, continuous time random walk (CTRW)(Berkowitz et al., 2001; Cortis et al., 2006; Mettier et al., 2006), and convolution-based particle tracking (CBPT)(Robinson et al., 2010). Particle tracking methods have been frequently adopted in the study of flow and solute transport in groundwater modeling. The most common applications are for the delineation of path lines in a flow model. Softwares have the module of particle tracking (MODFLOW), or provide a visualization tool for the path lines and travel times simulation (FEFLOW, ParaView).

One of the most popular applications of RWPT is to get pathlines for the average flow field. This is done by switching off the local dispersion, only introducing advection at various locations. Pathlines and travel times can be simulated and visualized.

In a research paper by Izbicki et al. (2004), ground-water flow model and particle tracking model were used to simulate the flow-path and time-of-travel results for the Mojave River ground-water basin. The simulation results were compared with isotopic data, in order to get a better understanding of the relation between surface flows in the river and ground-water in the floodplain aquifer.

Pint et al. (2003) simulated the flowpaths, travel times and capture zones in the Allequash Basin with MODFLOW and MODPATH. The simulation results agreed with the measurements of water source in the stream subsurface. In the flowpath analysis, particles were inserted below the creek streambed and tracked backward to their points of origin.

Robinson and Reay (2002) used MODFLOW and MODPATH to determine ground water flow patterns, discharge and recharge zones, and travel times in an unconfined ground water system. The particles were tracked back toward their point of origin into the ground water system. Recharge zones were determined, advective transport were simulated, but the effect of dispersive transport couldn't be accounted.

Sloan and Ewen (1999) developed a method to simulate the long-term migration of radionuclides in the near-surface of a river catchment. A particle tracking model was used for overland flow, which was characterized by a set of transfer functions. The travel times for particles released into the velocity field and then moved by advection determined the transfer functions.

Barber et al. (1996) evaluated the relationship between land-use changes and groundwater quality in a water-supply catchment. Pathlines and travel times of particles captured by production bores were estimated by reverse particle tracking from each bore.

North et al. (2008) studied the influences of vertical swimming behavior to dispersal of oyster larvae. A coupled particle-tracking and hydrodynamic model was used to predict the movement of particles based on advection, sub-grid scale turbulence and larval swimming behavior.

The statistical nature of the RWPT method makes it suitable to find bulk-averaged characteristics, for instance, the location of the contaminant plume, percentage of mass that crosses a boundary, etc., especially in the advection-dominated problems with infinite Peclet number.

Hassan and Mohamed (2003) used the particle tracking method to predict transport in

single continuum and dual continua (fractured systems) porous media. Their results showed that in the simulation of 2D problem with homogeneous conductivity and pulse contaminant injection the RWPT method matched the analytical solution better than the standard finite difference and finite element techniques because it did not suffer from numerical dispersion. They also analyzed the sensitivity of different factors such as the size of the support volume or projection area that was used to convert particle distribution to concentration values, time step size, and number of particles. In the simulation of matrix diffusion in fractured systems they found that the RWPT method could not get a delay in the arrival of the peak of the mass flux nor a tailing behavior of the breakthrough curves.

Suh (2004) presented a hybrid model with a neutral RWPT method adopted in the vicinity of the source point and Eulerian-Lagrangian concentration model in the far field to predict dispersion of heated water and suspended solids in coastal regions. The result showed that the random walk model was well suited for the region where the concentration gradients were high. But the author also recommended that RWPT be applied only in cases where it is absolutely necessary because the drawback of this method that adopting large number of particles is time consuming, and that the conversion from the particle number to concentration representation can produce numerical errors.

Israelsson et al. (2005) compared RWPT with two other Lagrangian approaches with potential use in extending near field mixing calculations. All these three methods can be used in both scale-dependent and constant diffusivity, but they are only applicable to computing mean concentrations. The authors concluded that RWPT is the most accurate one, capable of handling complexities in the flow field and domain geometry, but also the most computationally expensive one of these three approaches. RWPT can be applied to complex velocity or diffusivity fields, and no-flux and open boundary conditions. It also can be used for long-term simulations because it can visualize dominant transport pathways in complex flows.

Robinson et al. (2010) introduced a numerical technique CBPT - the convolution-based particle tracking to simulate resident or flux-averaged solute concentration in groundwater models which had a steady-state flow field with linear sorption and first order decay. The method is able to maintain sharp fronts for low-dispersion systems and accurately simulate the plume concentrations in an idealized test problem. The method can implement various

forms of dispersion tensor and has a parallel computing when a large number of particles are used in simulations.

Srinivasan et al. (2010) presented a combined CTRW-CBPT approach to simulate non-Fickian transport in three-dimensional macroscopically heterogeneous porous media.

Suk and Yeh (2010) presented a particle tracking technique that used a linear temporal interpolation scheme of the velocity field to account for the change in velocity during a time step in unsteady flow.

The RWPT method can also be adopted in reactive transport simulations, although normally it is only suitable for first order chemical kinetic processes.

Fernandez-Garcia and Sanchez-Vila (2011) presented a method to directly reconstruct the functional based on kernel density estimators to simulate reactive transport problems where the mixing of two different waters carried two chemical species and moved through a randomly heterogeneous porous medium.

1.2 Objective

Most of the researches using particle tracking method only considered the advective-dispersive process, few of them mentioned about retardation and decay. To this purpose, a RWPT model was established on a scientific software platform OpenGeoSys (OGS)(Kolditz and Bauer, 2004; Kolditz et al., 2012a,b) as discussed in the following section.

The OGS project is an open source initiative for numerical simulation of thermo-hydro-mechanical-chemical(THMC) processes in porous media. Finite element method was used for the calculation of the velocity field. In the RWPT simulation, a finite number of particles were injected into the calculation domain(Park et al., 2008b), the mobility of the particles was controlled by using retardation and decay models. The number of particles that leave the domain was counted to produce the breakthrough curves.

1.3 Dissertation organization

The dissertation is organized in the following structure. Chapter 2 presents the theory of flow and mass transport, and introduces the conception of random walk particle tracking.

Chapter 3 explains the implementation concept of the RWPT method in OGS, including the element search method, and boundary control method. Then the factors that can affect the efficiency and accuracy of the method are discussed. Parallel computing concept is included in the implementation. Chapter 4 presents the benchmarks developed for the RWPT method in OGS and compares the results with analytical solutions and other numerical methods to testify the presented method. Chapter 5 shows the ability of RWPT method in OGS to be adopted in different flow processes, e.g. Forchheimer flow and Richards flow. In chapter 6, two applications of the method are described. The first one is pore scale modeling which shows the capability of the method in describing details of transport process. The second one is a real application in Nankou catchment which is a 2D case study comparing homogeneous and heterogeneous material properties. Chapter 7 summarizes the work and gives outlook in the future.

Chapter 2

Theory

2.1 Flow and mass transport

In the simulation of flow and transport of contaminants in porous media, continuum soil physical concepts and theories are widely adopted. The concept of representative elementary volume (REV) (Bear, 1979) is introduced to represent a volume that within which the structure of the porous medium is neglected and the material parameters are averaged. The theories stated below are based on this REV concept.

2.1.1 Groundwater flow

To quantitatively describe groundwater flow in porous media, Darcy's law and the law of conservation of mass are considered.

Darcy's law was formulated by Henry Darcy based on experimental results of flow of water through a saturated soil column. Darcy found that if the soil column with the length $L\ [L]$ is set with hydraulic head of $h_A[L]$ and $h_B[L]$ on the inlet and outlet side respectively, then the volumetric flow rate $Q\ [L^3T^{-1}]$ in the column is proportional to the cross-sectional area of the column, $A\ [L^2]$, and the hydraulic gradient, ∇h,

$$Q = -KA(\frac{h_A - h_B}{L}) = -KA\nabla h \tag{2.1}$$

where $K\ [LT^{-1}]$ is hydraulic conductivity. The negative sign indicates the flow is to

the direction of decreasing hydraulic head. Division through A yields the equation of the volumetric flux q $[LT^{-1}]$

$$q = \frac{Q}{A} = -K\nabla h \tag{2.2}$$

The hydraulic conductivity K is introduced as a proportionality factor that is determined in experiment. It can be written as

$$K = k\frac{\rho g}{\mu} \tag{2.3}$$

where $k[L^2]$ is called intrinsic permeability, which is a parameter independent of the fluid, $\rho[ML^{-3}]$ is density of water, $g[LT^{-2}]$ is gravitational acceleration, and $\mu[MT^{-1}L^{-1}]$ is dynamic viscosity of water.

Equation (2.2) can also be expressed as

$$q = -\frac{k}{\mu}\nabla P \tag{2.4}$$

where ∇P is pressure gradient.

In an imaginary control volume, the difference between the mass of water entering the volume and the mass of water leaving the volume is balanced by a change in the mass of water stored in the volume. Assume that the dimensions of the volume is dx $[L]$, dy $[L]$ and dz $[L]$ in the x, y and z coordinate directions, respectively. The mass M_{in} $[M]$ with the density ρ $[ML^{-3}]$ entering the volume with volumetric flux q $[LT^{-1}]$ within a period of time dt $[T]$ is

$$M_{in} = \rho(q_x dydz + q_y dxdz + q_z dxdy)dt \tag{2.5}$$

and the mass M_{out} $[M]$ leaving the volume is

$$M_{out} = \rho[(q_x + \frac{\partial q_x}{\partial x}dx)dydz + (q_y + \frac{\partial q_y}{\partial y}dy)dxdz + (q_z + \frac{\partial q_z}{\partial z}dz)dxdy]dt \tag{2.6}$$

The net mass accumulation in the volume due to movement is given by

$$M_{in} - M_{out} = -\rho(\frac{\partial q_x}{\partial x} + \frac{\partial q_y}{\partial y} + \frac{\partial q_z}{\partial z})dxdydzdt \tag{2.7}$$

If the porous medium is saturated, then the change in the mass M $[M]$ stored in the volume with respect to time t $[T]$ can be expressed by

$$\frac{\partial M}{\partial t} = \frac{\partial}{\partial t}(\rho n dxdydz) \tag{2.8}$$

where n $[-]$ is porosity.

The net mass accumulation is equal to the change of mass with time

$$M_{in} - M_{out} = \frac{\partial M}{\partial t}dt \tag{2.9}$$

Substitute equation (2.7) and equation (2.8) into equation (2.9) yields

$$-\rho(\frac{\partial q_x}{\partial x} + \frac{\partial q_y}{\partial y} + \frac{\partial q_z}{\partial z})dxdydzdt = \frac{\partial}{\partial t}(\rho n dxdydz)dt \tag{2.10}$$

Division through $dxdydzdt$ simplifies

$$-\rho(\frac{\partial q_x}{\partial x} + \frac{\partial q_y}{\partial y} + \frac{\partial q_z}{\partial z}) = \frac{\partial(\rho n)}{\partial t} \tag{2.11}$$

The right hand side of equation (2.11) can be expanded as

$$\frac{\partial(\rho n)}{\partial t} = n\frac{\partial \rho}{\partial t} + \rho\frac{\partial n}{\partial t} \tag{2.12}$$

The two terms are the mass rate produced by expansion of the water under a change in its density and compaction of the porous medium reflected by a change in its porosity, respectively. Both of them are produced by the change of pressure P $[ML^{-1}T^{-2}]$. And the change of pressure is related to hydraulic head $h[L]$

$$dP = \rho g dh \tag{2.13}$$

The compressibility of water, $\beta[M^{-1}LT^2]$, is defined as the rate of change in density with regards to pressure

$$\beta dP = \frac{d\rho}{\rho} \tag{2.14}$$

Substitute equation (2.13) into equation (2.14) we have

$$d\rho = \rho\beta(\rho g dh) \tag{2.15}$$

The compressibility of porous medium, $\alpha[M^{-1}LT^2]$, is given by

$$\alpha dP = \frac{d(dz)}{dz} \tag{2.16}$$

Note that if the porous medium compresses or expands, the porosity will change, but the volume of the solids stays the same

$$d[(1-n)dxdydz] = 0 \tag{2.17}$$

Differentiation of the equation yields

$$dzdn = (1-n)d(dz) \tag{2.18}$$

and

$$dn = \frac{(1-n)d(dz)}{dz} \tag{2.19}$$

Substitute equation (2.16) and equation (2.13) into equation (2.19) yields

$$dn = (1-n)\alpha(\rho g dh) \tag{2.20}$$

Substitute equation (2.15) and equation (2.20) into equation (2.12) yields

$$\frac{\partial(\rho n)}{\partial t} = n\rho\beta\rho g\frac{\partial h}{\partial t} + \rho\alpha\rho g\frac{\partial h}{\partial t} \tag{2.21}$$

The storativity (volumetric specific storage), S_s $[L^{-1}]$, is defined as $S_s = \rho g(\alpha + n\beta)$. Substitute Darcy's law and equation (2.21)into equation (2.11) yields the governing equation of groundwater flow in a confined aquifer

$$\frac{\partial}{\partial x}(K_x\frac{\partial h}{\partial x}) + \frac{\partial}{\partial y}(K_y\frac{\partial h}{\partial y}) + \frac{\partial}{\partial z}(K_z\frac{\partial h}{\partial z}) = S_s\frac{\partial h}{\partial t} \tag{2.22}$$

2.1.2 Mass transport

Solute transport in porous media includes processes such as advection, molecular diffusion, hydromechanical dispersion, and retardation in a general sense.

- Advection

The advective transport is described by the average seepage velocity field as the solute is carried along with the flow of groundwater. Since the groundwater flow only occurs in the void space of the porous media, the actual flow velocity, i.e. the seepage velocity, v $[LT^{-1}]$, is related to the specific discharge q $[LT^{-1}]$

$$v = \frac{q}{n} \tag{2.23}$$

where n $[-]$ is porosity.

- Molecular Diffusion

Molecular diffusion describes the fact that a solute in the water always moves to the areas with low concentrations, no matter if there is fluid flow in existence. The mass of diffusing is proportional to the concentration gradient, known as Fick's first law

$$F = -D_d\frac{\partial C}{\partial x} \tag{2.24}$$

where $F[ML^{-2}T^{-1}]$ is the mass flux of solute per unit area per unit time, $D_d[L^2T^{-1}]$ is the diffusion coefficient, $C[ML^{-3}]$ is the solute concentration and $\frac{\partial C}{\partial x}[ML^{-3}L^{-1}]$ is the concentration gradient.

In systems where concentrations change with time, Fick's second law is applied

$$\frac{\partial C}{\partial t} = D_d\frac{\partial^2 C}{\partial x^2} \tag{2.25}$$

- Hydrodynamic Dispersion

The hydromechanical dispersion occurs when the flow velocity deviates locally from the average seepage velocity, which can be caused by pore sizes differences, pathlines, and frictional forces. Dispersion is always larger in flow direction than perpendicular to it. The hydromechanical dispersion coefficient D $[L^2T^{-1}]$ is expressed as follows

$$\begin{aligned} D_L &= \alpha_L v_i \\ D_T &= \alpha_T v_i \end{aligned} \tag{2.26}$$

where α_L is the longitudinal dispersivity $[L]$, α_T is the transverse dispersivity $[L]$.
The hydrodynamic dispersion includes both hydromechanical dispersion and diffusion.

- Advection-Dispersion Equation

The derivation of the advection-dispersion equation is based on the principle of mass conservation applied to a control volume.

The solute transported by advection and hydrodynamic dispersion can be expressed as $v_i n C dA$ and $nD_i \frac{\partial C}{\partial t} dA$, respectively. Where A $[L^2]$ is the cross-sectional area of the control volume and i direction is normal to that cross section. Advection and hydrodynamic dispersion are both linear so they can be superimposed, thus the total mass of solute transported per unit area is

$$F_i = v_i n C - n D_i \frac{\partial C}{\partial t} \tag{2.27}$$

The total mass of solute entering the control volume is

$$F_x dydz + F_y dxdz + F_z dxdy \tag{2.28}$$

and the total mass of solute leaving the control volume is

$$(F_x + \frac{\partial F_x}{\partial x})dydz + (F_y + \frac{\partial F_y}{\partial y})dxdz + (F_z + \frac{\partial F_z}{\partial z})dxdy \tag{2.29}$$

The net mass accumulation in the volume is

$$-(\frac{\partial F_x}{\partial x} + \frac{\partial F_y}{\partial y} + \frac{\partial F_z}{\partial z})dxdydz \tag{2.30}$$

The rate of mass change in the control volume is

$$n\frac{\partial C}{\partial t}dxdydz \tag{2.31}$$

Consider the law of mass conservation, the net mass accumulation in the volume is equal to the rate of mass change

$$-(\frac{\partial F_x}{\partial x}+\frac{\partial F_y}{\partial y}+\frac{\partial F_z}{\partial z})=n\frac{\partial C}{\partial t} \tag{2.32}$$

Substitute equation (2.27) into equation (2.32) yields

$$\frac{\partial C}{\partial t}=[\frac{\partial}{\partial x}(D_x\frac{\partial C}{\partial x})+\frac{\partial}{\partial y}(D_y\frac{\partial C}{\partial y})+\frac{\partial}{\partial z}(D_z\frac{\partial C}{\partial z})]-[\frac{\partial}{\partial x}(v_xC)+\frac{\partial}{\partial y}(v_yC)+\frac{\partial}{\partial z}(v_zC)] \tag{2.33}$$

which is the governing equation of mass transport for a conservative solute in porous media (Bear, 1979). If the Laplace operator is applied, the above equation can be written in a vector form as

$$\frac{\partial C}{\partial t}=\nabla\cdot(D\nabla C)-\nabla\cdot(\mathbf{v}C) \tag{2.34}$$

where C is the concentration (ML^{-3}), $\mathbf{v}$ is the pore velocity vector (ML^{-1}), and D is the hydrodynamic dispersion tensor (L^2T^{-1}), t is time (T^2), ∇ is the gradient operator, and $\nabla\cdot$ is the divergence operator.

2.2 Random walk particle tracking

The random walk particle tracking method is issued from stochastic physics. The stochastic differential equation is (Ito, 1951)

$$x(t_i)=x(t_{i-1})+\mathbf{v}(x(t_{i-1}))\Delta t+Z\sqrt{2D(x(t_{i-1}))\Delta t} \tag{2.35}$$

where x is the coordinates of the particle location, Δt is the time step, and Z is a random number whose mean is zero and variance is unity.

It has been shown that this equation is equivalent to an equation that is slightly different from the advection-dispersion Eq. (2.34). To be equivalent to Eq. (2.34), the modified velocity (Kinzelbach, 1986) and dispersion tensor (Bear, 1979) are expressed as

$$\mathbf{v}_i^* = \mathbf{v}_i + \sum_{j=1}^{3} \frac{\partial D_{ij}}{\partial x_j} \tag{2.36}$$

$$D_{ij} = \alpha_T |\mathbf{v}| \delta_{ij} + (\alpha_L - \alpha_T) \frac{\mathbf{v}_i \mathbf{v}_j}{|\mathbf{v}|} + D_{ii}^d \tag{2.37}$$

where δ_{ij} is the Kronecker symbol, α_L is the longitudinal dispersion length, α_T is the transverse dispersion length, D_{ij}^d is the tensor of molecular diffusion coefficient, and $\mathbf{v}_i$ is the component of the mean pore velocity in the ith direction.

The equivalent stochastic differential equation to Eq.(2.34) in three-dimensional problems can be written as (Kinzelbach, 1988; LaBolle et al., 1996; Tompson and Gelhar, 1990)

$$\begin{aligned}
x_{t+\Delta t} &= x_t + \left(\mathbf{v}_x(x_t, y_t, z_t, t) + \tfrac{\partial D_{xx}}{\partial x} + \tfrac{\partial D_{xy}}{\partial y} + \tfrac{\partial D_{xz}}{\partial z} \right) \Delta t \\
&\quad + \sqrt{2D_{xx}\Delta t} Z_1 + \sqrt{2D_{xy}\Delta t} Z_2 + \sqrt{2D_{xz}\Delta t} Z_3 \\
y_{t+\Delta t} &= y_t + \left(\mathbf{v}_y(x_t, y_t, z_t, t) + \tfrac{\partial D_{yx}}{\partial x} + \tfrac{\partial D_{yy}}{\partial y} + \tfrac{\partial D_{yz}}{\partial z} \right) \Delta t \\
&\quad + \sqrt{2D_{yx}\Delta t} Z_1 + \sqrt{2D_{yy}\Delta t} Z_2 + \sqrt{2D_{yz}\Delta t} Z_3 \\
z_{t+\Delta t} &= z_t + \left(\mathbf{v}_z(x_t, y_t, z_t, t) + \tfrac{\partial D_{zx}}{\partial x} + \tfrac{\partial D_{zy}}{\partial y} + \tfrac{\partial D_{zz}}{\partial z} \right) \Delta t \\
&\quad + \sqrt{2D_{zx}\Delta t} Z_1 + \sqrt{2D_{zy}\Delta t} Z_2 + \sqrt{2D_{zz}\Delta t} Z_3
\end{aligned} \tag{2.38}$$

where x, y, and z are the coordinates of the particle location, Δt is the time step, and Z_i is a random number whose mean is zero and variance is unity.

In Eq. (2.38), the spatial derivatives of the dispersion coefficients are introduced from the modified velocity (Kinzelbach, 1986). Together with Eq. (2.37), the spatial derivatives of the dispersion coefficients can be expressed as a function of the derivatives of velocity. Note that to obtain the derivatives of velocity, velocity has to be continuous mathematically. To this end, we interpolate velocity at any location in an element from the known velocity at the element nodes. The velocity estimation and the interpolation method are provided in section 3.1.

Since the proposed RWPT method makes use of the FEM for velocity estimation, the

derivative of velocity within each element is computed as in Fig. 2.1 and written as

$$\begin{aligned} \frac{\partial \mathbf{v}_x}{\partial x} = \frac{\mathbf{v}(x_R)-\mathbf{v}(x_L)}{l_x}; \quad \frac{\partial \mathbf{v}_y}{\partial y} = \frac{\mathbf{v}(y_U)-\mathbf{v}(y_D)}{l_y}; \quad \frac{\partial \mathbf{v}_z}{\partial z} = \frac{\mathbf{v}(z_N)-\mathbf{v}(z_S)}{l_z} \\ \frac{\partial \mathbf{v}_x}{\partial y} = \frac{\partial \mathbf{v}_x}{\partial z} = \frac{\partial \mathbf{v}_y}{\partial z} = \frac{\partial \mathbf{v}_y}{\partial x} = \frac{\partial \mathbf{v}_z}{\partial x} = \frac{\partial \mathbf{v}_z}{\partial y} \simeq 0 \end{aligned} \tag{2.39}$$

where x_L and x_R are intersection points of the element edges with a line parallel to the global x axis at which velocities are $\mathbf{v}(x_L)$ and $\mathbf{v}(x_R)$, y_D and y_U are intersection points of the element edges from down to up with a line parallel to the global y axis at which velocities are $\mathbf{v}(y_D)$ and $\mathbf{v}(y_U)$, z_S and z_N are the intersection points of the element edges from south to north with a line parallel to the global z axis at which velocities are $\mathbf{v}(z_S)$ and $\mathbf{v}(z_N)$, and l_x, l_y, and l_z are the length of each intersection line, respectively.

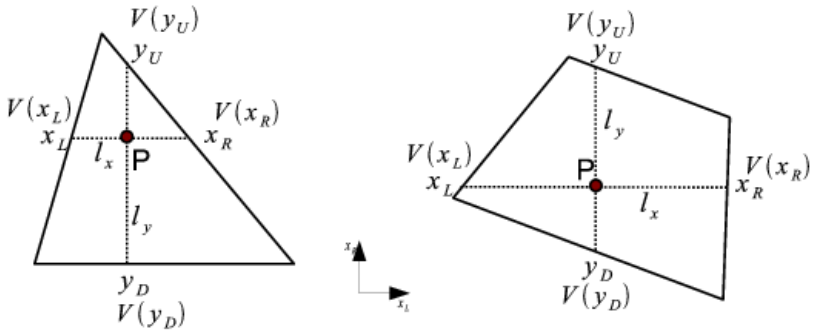

Figure 2.1: Spatial derivatives of velocity for a particle in triangular and quadrilateral elements

Thus, the derivatives of the dispersion coefficients are as follows (Hoteit et al., 2002)

$$
\begin{aligned}
\frac{\partial D_{xx}}{\partial x} &= \mathbf{v}_x \frac{\partial \mathbf{v}_x}{\partial x}\left[\alpha_L\left(\frac{2}{\mathbf{v}} - \frac{\mathbf{v}_x^2}{\mathbf{v}^3}\right) - \alpha_T \frac{\mathbf{v}_y^2+\mathbf{v}_z^2}{\mathbf{v}^3}\right] \\
\frac{\partial D_{xy}}{\partial y} &= (\alpha_L - \alpha_T)\left[\frac{\partial \mathbf{v}_y}{\partial y}\frac{\mathbf{v}_x}{\mathbf{v}} - \frac{\mathbf{v}_x \mathbf{v}_y^2}{\mathbf{v}^3}\frac{\partial \mathbf{v}_y}{\partial y}\right] \\
\frac{\partial D_{xz}}{\partial z} &= (\alpha_L - \alpha_T)\left[\frac{\partial \mathbf{v}_z}{\partial z}\frac{\mathbf{v}_x}{\mathbf{v}} - \frac{\mathbf{v}_x \mathbf{v}_z^2}{\mathbf{v}^3}\frac{\partial \mathbf{v}_z}{\partial z}\right] \\
\frac{\partial D_{yy}}{\partial y} &= \mathbf{v}_y \frac{\partial \mathbf{v}_y}{\partial y}\left[\alpha_L\left(\frac{2}{\mathbf{v}} - \frac{\mathbf{v}_y^2}{\mathbf{v}^3}\right) - \alpha_T \frac{\mathbf{v}_x^2+\mathbf{v}_z^2}{\mathbf{v}^3}\right] \\
\frac{\partial D_{yx}}{\partial x} &= (\alpha_L - \alpha_T)\left[\frac{\partial \mathbf{v}_x}{\partial x}\frac{\mathbf{v}_y}{\mathbf{v}} - \frac{\mathbf{v}_y \mathbf{v}_x^2}{\mathbf{v}^3}\frac{\partial \mathbf{v}_x}{\partial x}\right] \\
\frac{\partial D_{yz}}{\partial z} &= (\alpha_L - \alpha_T)\left[\frac{\partial \mathbf{v}_z}{\partial z}\frac{\mathbf{v}_y}{\mathbf{v}} - \frac{\mathbf{v}_y \mathbf{v}_z^2}{\mathbf{v}^3}\frac{\partial \mathbf{v}_z}{\partial z}\right] \\
\frac{\partial D_{zz}}{\partial z} &= \mathbf{v}_z \frac{\partial \mathbf{v}_z}{\partial z}\left[\alpha_L\left(\frac{2}{\mathbf{v}} - \frac{\mathbf{v}_z^2}{\mathbf{v}^3}\right) - \alpha_T \frac{\mathbf{v}_x^2+\mathbf{v}_y^2}{\mathbf{v}^3}\right] \\
\frac{\partial D_{zx}}{\partial x} &= (\alpha_L - \alpha_T)\left[\frac{\partial \mathbf{v}_x}{\partial x}\frac{\mathbf{v}_z}{\mathbf{v}} - \frac{\mathbf{v}_z \mathbf{v}_x^2}{\mathbf{v}^3}\frac{\partial \mathbf{v}_x}{\partial x}\right] \\
\frac{\partial D_{zy}}{\partial y} &= (\alpha_L - \alpha_T)\left[\frac{\partial \mathbf{v}_y}{\partial y}\frac{\mathbf{v}_z}{\mathbf{v}} - \frac{\mathbf{v}_z \mathbf{v}_y^2}{\mathbf{v}^3}\frac{\partial \mathbf{v}_y}{\partial y}\right]
\end{aligned}
\tag{2.40}
$$

Because velocity is not derivable at the interface of two adjacent elements in a nonuniform flow, computing dispersion coefficient derivatives by using a finite element approach would yield erroneous values (Hoteit et al., 2002). To prevent these errors, a particle is coded to have information of an element index and the velocity estimation is continuous even at the elemental boundaries in this method. Thus, the derivatives of dispersion coefficients will be computed accordingly. This is an improved approach from the work by Hoteit et al. (2002).

Chapter 3

Method implementation

3.1 Implementation concept

Random walk particle tracking method (RWPT) provides a computationally effective way to characterize solute transport process in porous media. In this work, a scientific software platform OpenGeoSys (OGS) was adopted for the simulation and visualization of the complex behaviors of particles. The OGS project is an open-source initiative for numerical simulation of thermo-hydro-mechanical/chemical (THM/C) processes in porous and fractured media for applications in geoscience and hydrology. It is based on object-oriented finite element method (FEM) concept to solve for multifield problems, including a broad spectrum of interfaces for pre- and postprocessing (Kolditz and Bauer, 2004; Kolditz et al., 2012b; Shao, 2010; Sun, 2011; Watanabe, 2012). All the work presented in this dissertation is based on OGS, and several benchmarks regarding RWPT are developed.

As presented in the previous chapter, the governing equations in the simulation of solute transport in porous media mainly consist of flow and mass transport equations. In this work, the flow equation is solved by FEM method and the transport equation is treated by RWPT method. This section aims to present the implementation of both the determination of velocity field and the interpolation of velocity for the transport.

In this work, finite element method is used for the calculation of the velocity field which is necessary for the determination of the displacement of the particles through space. The accuracy of the velocity field calculation is crucial to the precision of the RWPT method.

In the numerical simulation of groundwater flow, the hydraulic head distribution is numerically described by groundwater flow equation. According to Darcy's law, the velocity field is calculated from the hydraulic head difference. The standard FEM estimates the flow velocity on the element level, so discontinuities may occur at the element boundaries. A global node-based method was proposed (Park et al., 2008a; Yeh, 1981) to resolve the discontinuity problem. In this method, the Darcy velocity is solved using the Galerkin method that it is integrated on the domain and can be interpolated to any position.

Note that the velocity determination is necessary for but independent of the particle tracking process. In chapter 5 shows the flexibility of the RWPT method to be implemented with different kinds of flow processes.

After the velocity field is determined, the next step is the calculation of solute transport. In which way the velocities are used is the major difference between the particle tracking method and other numerical methods. The velocities of the particles are interpolated from the known points to the particles' locations and used directly for advecting the particles.

In the OGS framework, the dependency graph for the file "rf_random_walk.cpp" is shown in Fig. 3.1.

The collaboration diagram for the class "RandomWalk" is shown in Fig. 3.2.

The brief workflow of this process is sketched in Fig. 3.3. All the particles are independent from each other. Within each time step, each particle is looped over. First, the properties of the particle (e.g. element index information, coordinates, identity, velocity) in the last location are read from the memory. Then the displacement of the particle within this time step is calculated according to the velocity field, and the new location of the particle is obtained according to the equations mentioned in section 2.2. Next, an element search approach is applied to get the new index information of element in which the particle is located, which will be described in the next section. If the new index information can't be obtained, it means that the particle is outside of the calculation domain, and then a boundary control approach will be applied to "drag" the particle back to the surface of the domain, which will also be described in details in the next section of this chapter. With this new element index information, all the properties of the particle can be updated and written to the memory.

The particle has a property named "identity", which is a parameter with the value 0, 1,

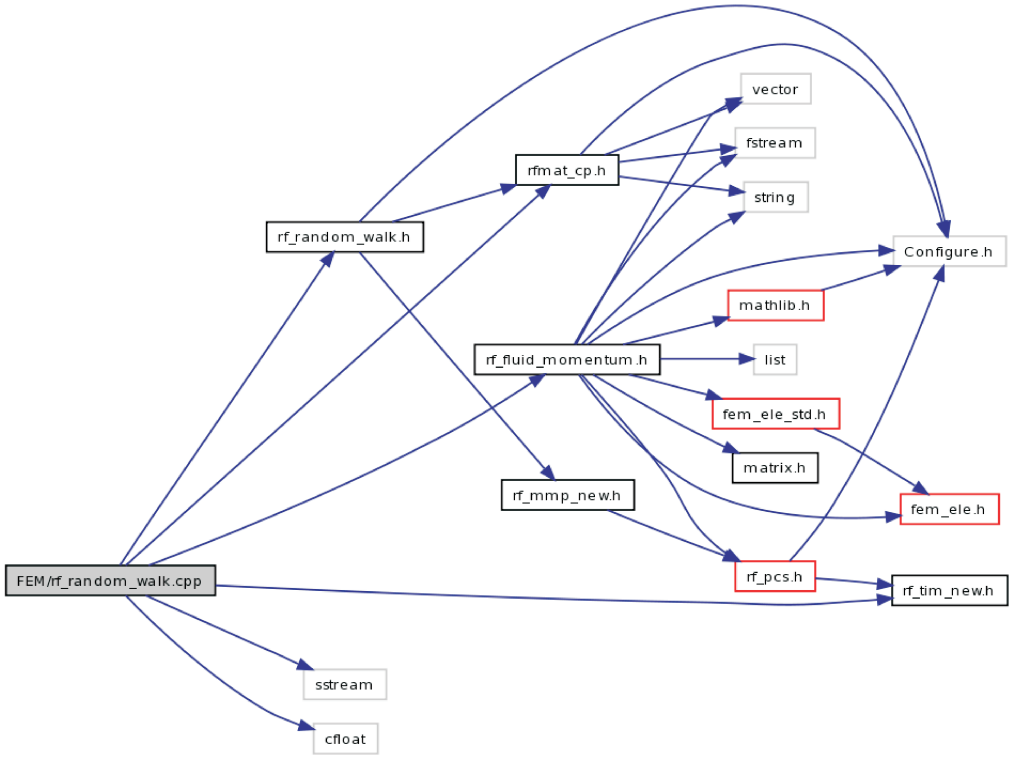

Figure 3.1: Dependency of the file rf_random_walk.cpp

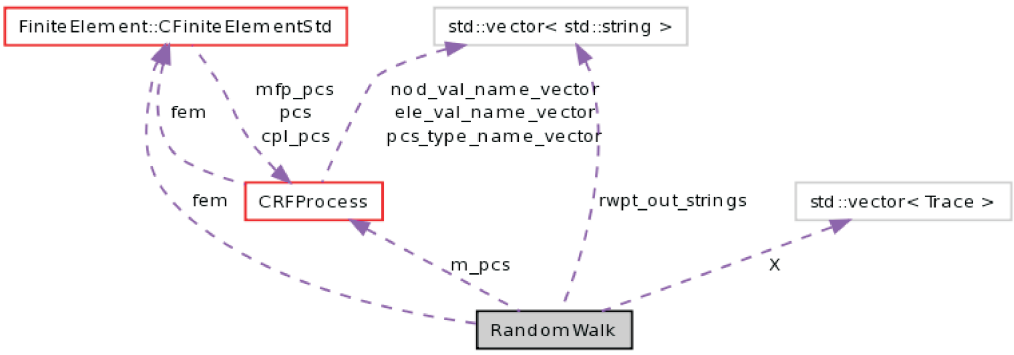

Figure 3.2: Collaboration of the class RandomWalk

or 2. When the particle is mobile, or free in the flow field, its identity is 0. If the particle is absorbed by the soil grain surface, its identity changes into 1. But the particle still has the chance to leave the surface of the grain and go back to the flow (so called desorption). If a particle is terminated by the filtration process, its identity changes to 2 and will never move again. In other words, particles with identity of 0 can go through the advection loop mentioned above, while particles with identity 1 go directly to the sorption-desorption and retardation processes.

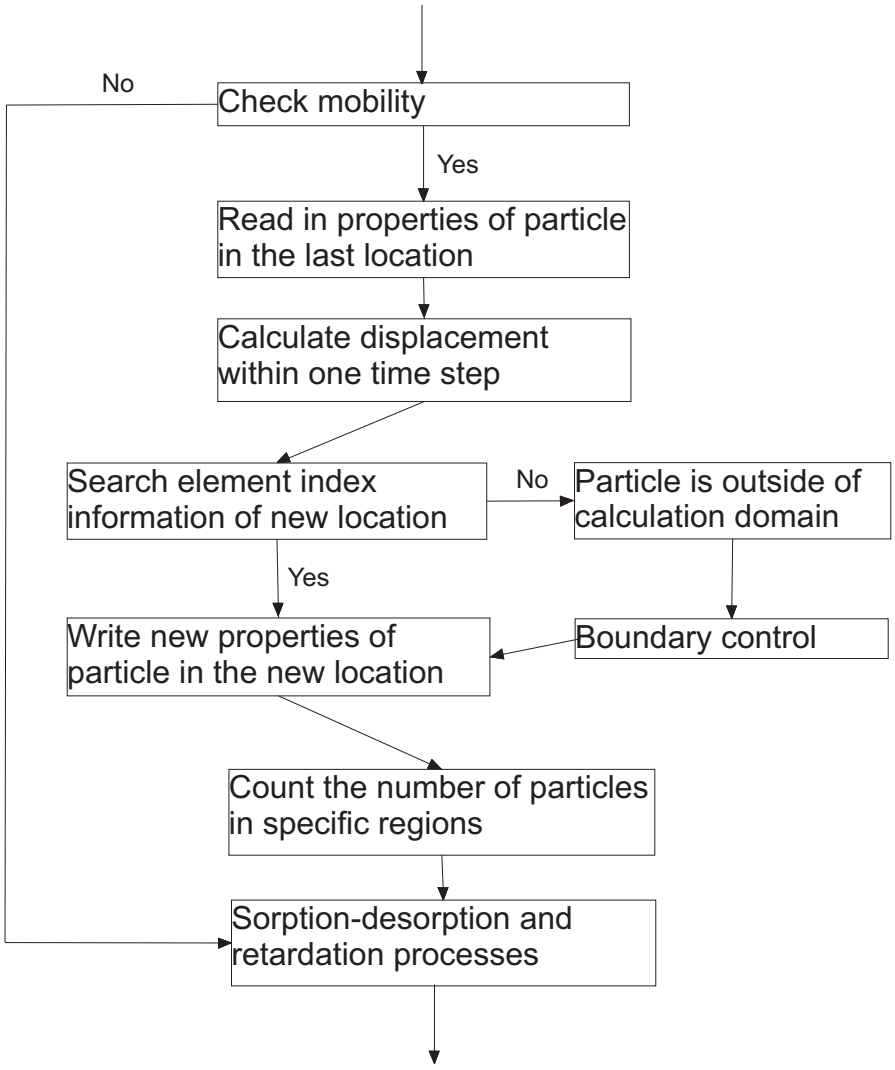

Figure 3.3: Workflow of particle tracking within one time step

3.2 Search Methods

3.2.1 Search element

In the RWPT method, at every time step for each particle it is necessary to know where the particle is, i.e., in which element is the particle located. Only then can we interpolate the velocity for the particle from the nodes of this element.

There are many classical algorithms to locate a specific position in a domain. For example, tree data structure, including binary trees, binary space partitioning (BSP) trees and so on. In the binary tree structure (Fig. 3.4), each parent node has two children nodes which contain references to it. All the nodes in the structure can be reached by following the references. Quadtree (Fig. 3.5) is a kind of BSP, often used to partition a two dimensional domain by subdividing it into four quadrants. Similarly, octree (Fig. 3.6) is used in three dimensional domain to subdivide the domain into eight octants.

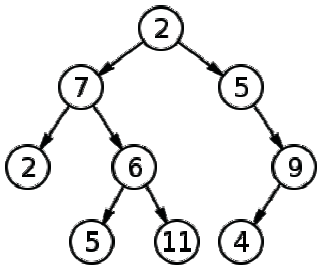

Figure 3.4: Sketch of binarytree data structure (source: wikipedia)

In this work, two algorithms are used for the particle position searching. The time consumption for testing benchmarks with different algorithms are compared. In 2D case, a square domain with the dimension of 100 by 100, discretized with quadrilateral elements (900) and triangular elements (882) are tested respectively.

- **Search all elements by index**

  With the quadrilateral elements, if the elements are searched by index, i.e. from element with index 0 to the one which contains the particle, there's a risk to search all of the 900 elements. Computation time is increasing rapidly when the number

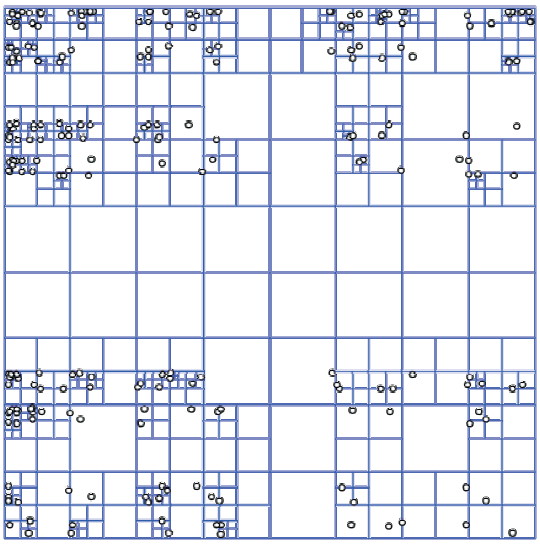

Figure 3.5: Sketch of quadtree data structure (source: wikipedia)

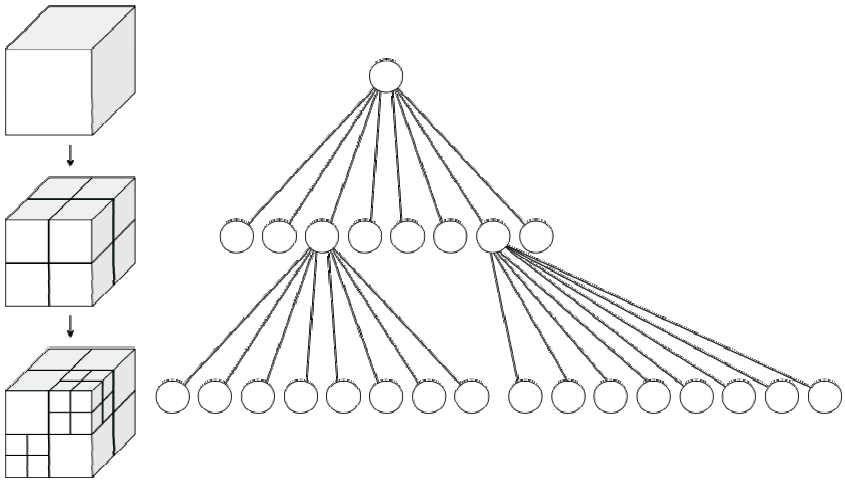

Figure 3.6: Sketch of octtree data structure (source: wikipedia)

of particles is increased. The result is shown by red curve with square symbols in Fig. 3.7(all quad - intersection).

- **Search elements from neighbours**

  If the elements are searched by neighbours, i.e. only the neighbour elements of the last position are searched, there's a chance that only a few elements are searched. Time consumption is shown by blue curve with square symbols in Fig. 3.7(neighbour quad - intersection).

With the triangular elements, similar results are shown by curves with delta symbols respectively in Fig. 3.7(all tri - intersection and neighbour tri - intersection).

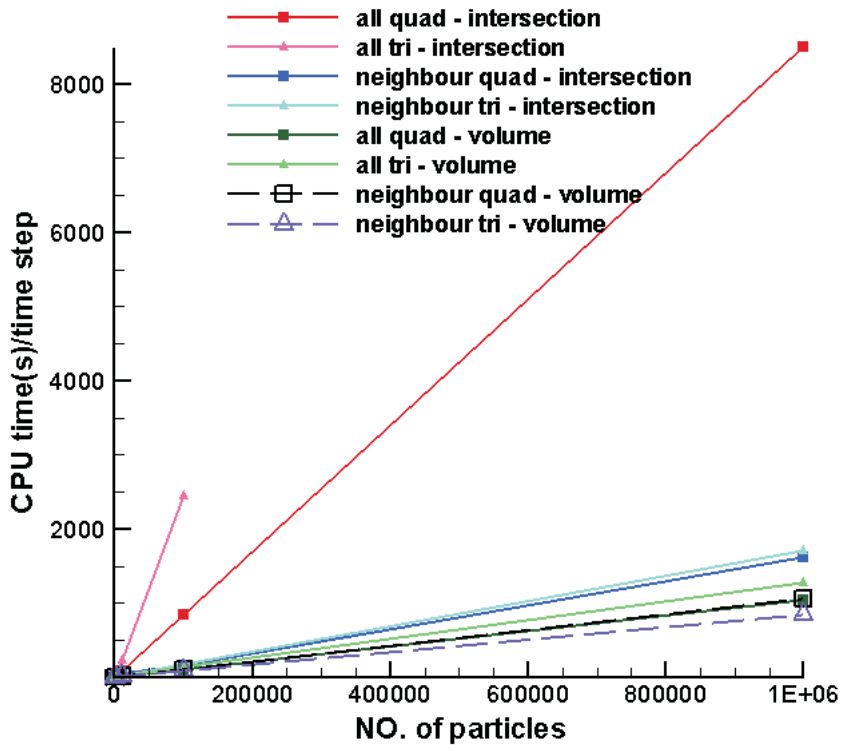

Figure 3.7: Time needed with different algorithms (2D elements)

In 3D case, a cube domain with the dimension of 1 by 1 by 1, and discretized with tetrahedral elements (5963) and prismatic elements (5700) are tested respectively. Results are shown in Fig. 3.8.

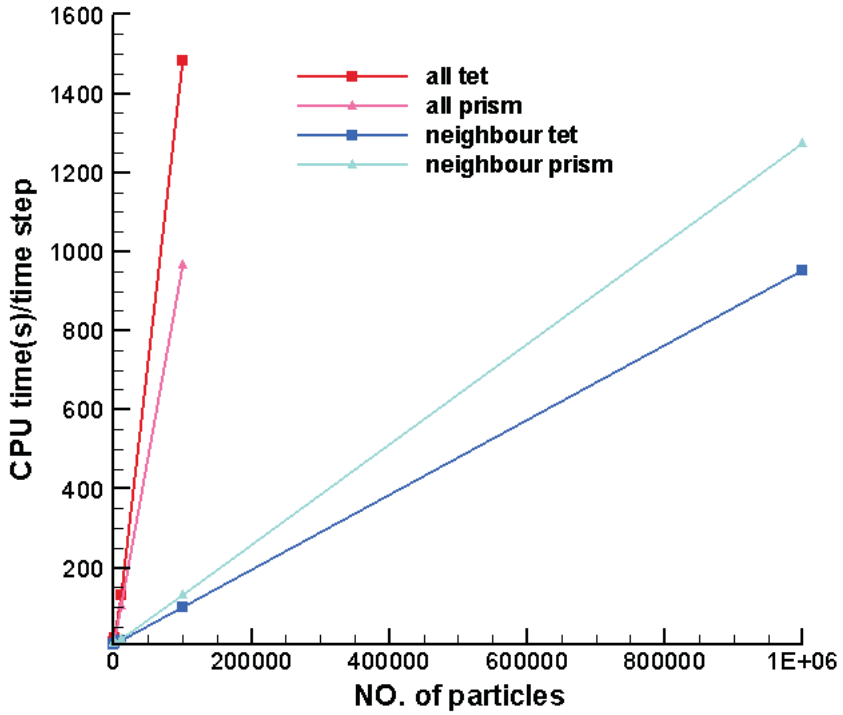

Figure 3.8: Time needed with different algorithms (3D elements)

3.2.2 Inside or outside criterion

Among several criterion to judge whether the specific position is inside or outside of the element, the “extension-line-intersection-criterion” and the “area/volume-compare-criterion” are discussed here.

- **Extension-line-intersection-criterion**

  In 2D case, first we pick an edge of this element; the two nodes of the edge are named P1 and P2 (Fig. 3.9). The position of the particle is named P3. Now we add a fourth point P4 which is far away in the x direction from P3. Thus two straight line segments L1 and L2 are formed by P1 and P2, P3 and P4, respectively.

  Next, we calculate the intersection of L1 and L2. Two line segments have four kinds of position relationships: collinear, parallel, intersect, and intersect in extension. In this case, it only counts when the two line segments intersect.

  Loop over all the edges of this element and count the number of intersection points. If the number is odd, then the particle is inside of this element.

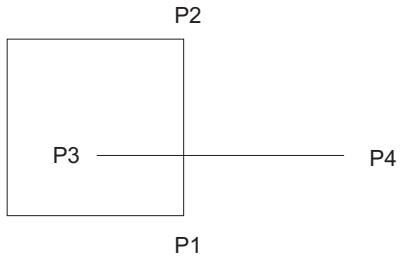

Figure 3.9: Schematic of extension-line-intersection-criterion

- **Area/volume-compare-criterion**

  In 2D case, first we pick an edge of this element; the two nodes of the edge are named P1 and P2 (Fig. 3.10). The position of the particle is named P3. Calculate the area of the triangle consists of P1, P2 and P3.

  Loop over all the edges of this element, and add all the triangles' area together. Compare the result with the area of the element, if the two equal, then the particle is inside of this element.

  In 3D case, calculate the volume of the tetrahedral consists of the particle and three nodes of the elements, add all together, and compare the result with the volume of the element, if the two equal, then the particle is inside of this element.

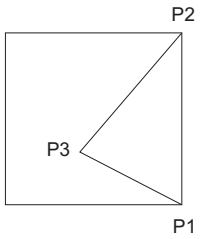

Figure 3.10: Schematic of area/volume-compare-criterion

Here we show that with the “area/volume-compare-criterion”, even if it has to search all the elements by index, time consumption is even less than the search neighbour method with “extension-line-intersection-criterion”. Result for the quadrilateral elements is shown by dark green curve with square symbols in Fig. 3.7(all quad - volume). Result for the triangular elements is shown by light green curve with delta symbols (all tri - volume).

If we combine the search neighbour method with the “area/volume-compare-criterion”, improvements can be found as shown with dashed lines in Fig. 3.7(neighbour quad - volume and neighbour tri - volume).

3.2.3 Boundary control

In the process of velocity interpolation for the transport, each particle obtains its velocity from its location and advects according to that velocity. If the particle is close to the boundary, there is a chance that the calculated displacement within one time step is bigger than the distance between the particle and the boundary. In this case, the calculated new location is actually outside of the calculation domain. In this work, a boundary control approach is applied that when the particle goes out of the calculation domain, it is ”dragged” back to the intersection point of its pathline and the boundary.

The basic idea of boundary control is to get the new location of the particle according to the old location and the displacement, find which element is the new location located in, if no element is found, i.e., the particle is outside of domain, calculate the intersection point between the path line and the boundary surface and drag the particle to the intersection point. If the old location is already on the boundary and the new location is outside of domain, drag it back without calculation. Note that particles on the boundary still have

chance to move or detach in the next time step. Illustration of the result after boundary control is applied is shown in Fig. 3.11.

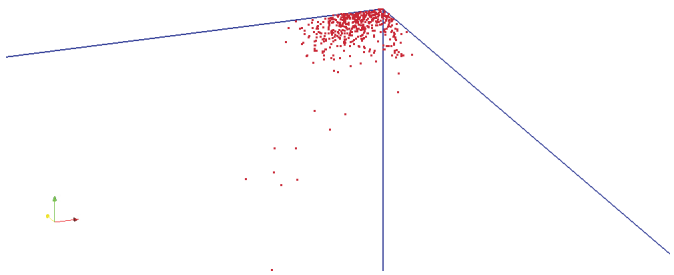

Figure 3.11: Illustration of boundary control

3.3 Accuracy and efficiency

The accuracy of the proposed RWPT method mainly depends on the total number of particles injected. The efficiency of the method depends on both the total number of particles injected and the total number of mesh nodes or elements.

3.3.1 Number of particles injected

As mentioned in the first chapter, one of the limitations of the RWPT method is that the computed concentrations have random fluctuations. The relative size of these fluctuations can be diminished by increasing the number of the particles. Several benchmarks support this point of view. For example, in Harter's experiment (see Section 4.1), which is a one dimensional groundwater flow with constant contamination injection with sorption-desorption and decay processes, the simulation results from using various numbers of injected particles are shown in Fig. 3.12.

If 250 particles are injected, which means 10 particles are injected for each time step, it is very hard to get a general idea of the breakthrough curve. If the number increase tenfold, tend of the breakthrough curve can be observed a little bit. When the number reaches

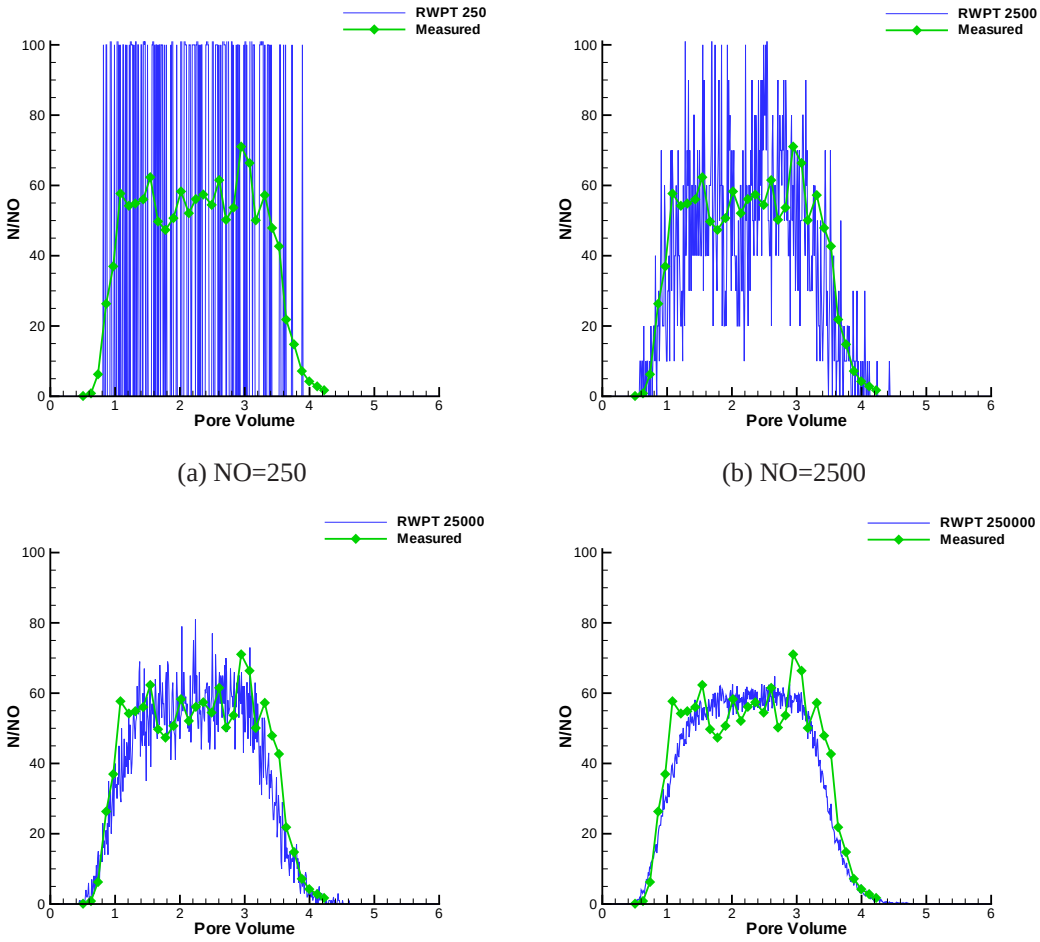

(a) NO=250

(b) NO=2500

(c) NO=25000

(d) NO=250000

Figure 3.12: Various numbers of injected particles for Harter's experiment

25000, it is almost comparable to the analytical solutions. Apparently, if the number keeps increasing to 250000, the breakthrough curve becomes very smooth.

But note that the increasing of particles number raises the demand of computation time. Within each time step, each particle is looped over to calculate its properties such as element index information, velocity, coordinates, and identity. It is obvious that the computation time is proportional to the number of iterations, which equals to the total number of particles. Several benchmarks are tested and the results are shown below.

Fig. 3.13 shows the relationship between the number of injected particles and the simulation time consumption in a one dimensional case (Harter's experiment, see Section 4.1). The calculation domain is discretized with line elements.

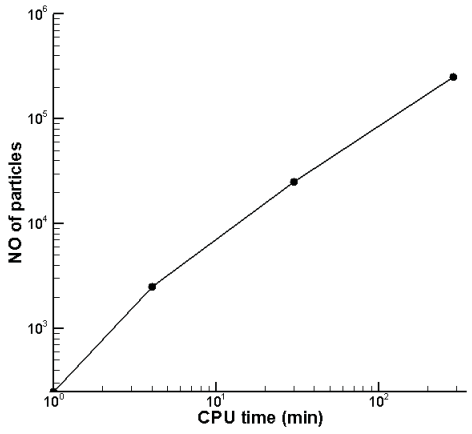

Figure 3.13: Time needed for Harter's experiment

Fig. 3.14 shows the relationship between the number of injected particles and the simulation time consumption in a three dimensional case (see Section 4.5). The calculation domain is discretized with tetrahedral elements.

Fig. 3.15 shows the relationship between the number of injected particles and the simulation time consumption in a three dimensional pore space case (see Section 4.7). The calculation domain is discretized with tetrahedral elements.

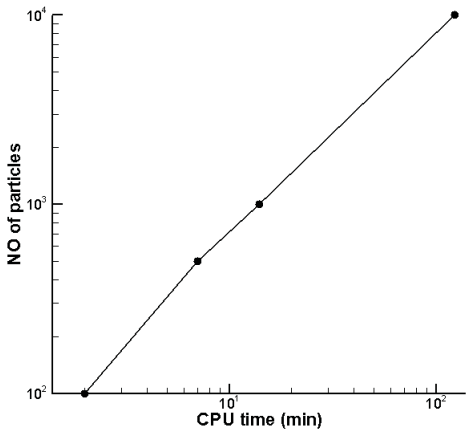

Figure 3.14: Time needed for 3D cube

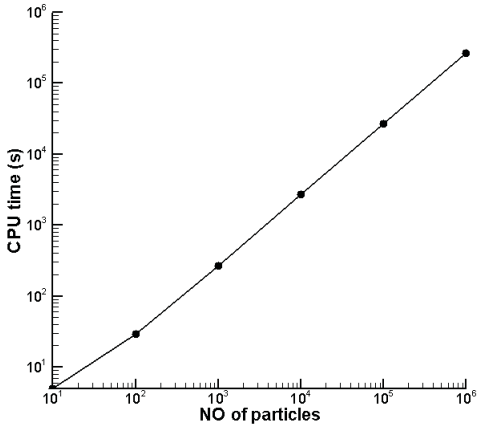

Figure 3.15: Time needed for 3D cube with one grain

3.3.2 Number of mesh nodes or elements

The number of nodes or elements of the mesh is another factor that affects the efficiency of the proposed RWPT method.

The grid Peclet number is the ratio of the typical advective velocity times the grid size divided by the dispersion coefficient. The proposed RWPT method does not have the restriction of Peclet number, thus relatively coarse mesh can be adapted, especially in advective-dominated problems.

In the particle tracking method, there is no potential requirement for fine mesh, because particles make use of the velocity field by interpolating from known points. But in the numerical simulation of groundwater flow, fine mesh or locally mesh refinement is always required for better resolution of the geometry. It is obviously that fine mesh can lead to the increment of computational time. In the proposed RWPT method, for each particle in each time step, the information of in which element the particle is located is necessary for the computing of particle's displacement. In the search element approach, if within one time step, the particle moves to a location that is not in the neighboring element of the last location, it takes much more efforts to search for the element index information.

3.4 Parallelization

As discussed in the last section, the main factors that affect the efficiency of the proposed RWPT method are the number of particles injected and the total number of the mesh elements or nodes. Since all the particles are isolated, i.e. the calculation of particles' displacements is operated separately from each other; it is ideally to use parallel computing to enhance the computational efficiency. Concerning the factor of the total number of the mesh elements or nodes, domain decomposition is a good option.

3.4.1 Parallel computing

The development of high performance computers makes it possible to deal with complex problems efficiently, in the manner of parallel computing. Parallel computing is a form of computation in which calculations are divided into several discrete parts which can

be carried out simultaneously. A computational problem can be parallelized if it is able to be broken apart, and execute multiple program instructions at any moment in time. The computation time spent in parallel computing should be less than that when the problem is solved with single computer.

Types of parallelism include bit-level, instruction level, data, and task parallelism. The bit-level parallelism refers to the double of computer word size, which is achieved by the development of computer-chip fabrication technology that for example 4-bit microprocessors were replaced by 8-bit, et cetera. Instruction level parallelism means that a stream of instructions can be re-ordered and combined together to be executed in parallel by a single processor. Data parallelism is also known as loop-level parallelism, which focuses on distributing the data across different parallel computing nodes. On the contrast, task parallelism, also known as function parallelism or control parallelism, focuses on distributing execution processes rather than data.

Concerning the hardware, parallel computers can be divided into multi-core and multiprocessor computers with multiple processing elements in a single machine, and multiple computers such as clusters. Memories in parallel computers have three types, shared memory, distributed memory, and shared distributed memory. Shared memory can be simultaneously accessed by multiple programs as global address space. Changes in a memory location effected by one program are visible to all other programs. Distributed memory is private for the programs and requires a communication network to connect inter-processor memory. Shared distributed memory is the combination of both.

Concerning the software, concurrent programming languages, libraries, application programming interface (API), and parallel programming models have been created, which can be divided into groups according to the fundamental memory architectures they are based on, i.e., shared memory, distributed memory, and shared distributed memory. Commonly used parallel programming models include shared memory, distributed memory, threads, data parallel, hybrid, single program multiple data and multiple program multiple data.

Communication and synchronization between different discrete parts are the most important issues in the performance of parallel computing. Communication refers to the data

exchange between parallel tasks, and can be effected by several factors, for instance, latency, bandwidth, visibility of communications, cost of communications, scope of communications and efficiency of communications. Synchronization refers to the coordination of parallel tasks in real time. Commonly used synchronization method includes barrier, lock/semaphore, and synchronous communication operations.

Amdahl's law (Amdahl, 1967) describes the potential speed-up of a program on a parallel computing platform. If α is the fraction of computational time spent on non-parallelized parts, then the speed-up S is given by

$$S = \frac{1}{\alpha} \tag{3.1}$$

Gustafson's law states that with P processors the speed-up of a program S is given by

$$S(P) = P - \alpha(P - 1) \tag{3.2}$$

3.4.2 Domain decomposition

Domain decomposition is a method that solves a problem by splitting the calculation domain into several sub-domains, solving problem on each sub-domain, and combing them together to get the solution to the problem on the original domain. The potential assumptions include that the problems on sub-domains are independent and can be solved with concurrency, the solution on sub-domains are easier than that on the original domain. Domain decomposition is used in parallel computing to decompose the data rather than the tasks, the latter is known as functional decomposition. In this type of partitioning, the data is decomposed and each task works on a portion of the data.

Domain decomposition methods can be divided into two groups according to the manner how the sub-domains intersect: overlapping method and non-overlapping method. The former one is represented by the Schwarz method and the latter by Schur complement method, and primal methods such as balancing domain decomposition (BDD) and dual methods such as finite element tearing and interconnect (FETI).

In this work, the finite element method is parallelized based on the domain decomposition concept (DDC). The computational domain is topological discretized into sub-domains, on which the finite element contributions are assembled, and then the sub-domain contributions are reconciled to obtain the solution on the original domain. Three basic steps are included in the parallelization concept: domain decomposition, partitioning of global equation systems, and partitioning of the global linear solver.

In the domain decomposition, Schur complement method is adopted that sub-domains intersect only on their interface, thus the assembly of element matrices and vectors are restricted to sub-domains. The computational mesh domain is decomposed by the software METIS (Karypis and Kumar, 1998). Normally the number of sub-domains is corresponding to the processors of the parallel computer. The sub-domains contain global element indices, and internal and border nodes. All these information are stored in a DDC file that is prepared by METIS. The DDC file is read as well as the mesh file, and then the parallel computation is operated on each sub-domain. The global equation system is separated into local equation systems according to the domain decomposition, and the local equation systems are cast to the processors concurrently. Global data is mapped to local data so that local equation systems can be established by assembling matrices and vectors for each element on the sub-domain. Concerning the partitioning of global linear solver, an iterative Krylov solver method is modified to carry out the matrix-vector-multiplications on sub-domain level. Details of parallel finite element method in the OGS are described by Wang et al. (2009).

3.4.3 Data parallelism

Data parallelism is also known as loop-level parallelism, in which each processor executes the same task on different part of the data simultaneously.

Among various methods, Open Multi-Processing (OpenMP) is one of most widely used APIs, which supports shared memory programming in C, C++, and Fortran, on most processor architectures and operating systems. It is composed by three primary API components: compiler directives, runtime library routines, and environment variables. It is designed for shared memory model that all threads have access to the same memory. Shared

data is accessible by all threads, while private data is only accessible by the thread that owns it. It is a fork-join model that all programs begin with the so-called master thread, which executes sequentially, and then go to the parallel region where the master thread creates a number of so-called work threads. After all the work threads have been executed in parallel and synchronized, they joined together to form the master thread again.

OpenMP is focus to parallelize loops. It provides a set of ”pragmas” for the compiler to parallelize the source codes without significantly rewrite them. In the parallel region, if the pragmas are supported by the compiler, then a block of source code is executed by all threads simultaneously. If not, the program will ignore the pragma and still yield correct behavior without parallelism.

The general steps to apply OpenMP to the source code are to insert appropriate pragmas in the source code, and build the program with an OpenMP-capable compiler. The compiler interprets the pragmas and parallelizes the code that following the pragma. The ”parallel pragma” creates a number of work threads, all of which execute the block of source code that follows simultaneously until the end of the block, and join back into the master thread. The ”for pragma” splits the for-loop so that each thread handles a different section of the loop and executes in parallel.

In this work, the ”for pragma” is applied in the section where the particle information such as velocity, displacement, element index and mobility of the particles is calculated. The calculation and update of particle information are independent of each other. With this parallelism, each thread can handle a number of particles and calculate in parallel.

Chapter 4

Benchmarks

4.1 RWPT in homogeneous porous medium: 1D case study

4.1.1 Definition

A one-dimensional homogeneous aquifer is chosen to simulate a soil column experiment conducted by Harter and Wagner (2000). In the experiment, a constant flow rate was established, 2.5 pore volumes NaCl - tap water solution and 2.5 pore volumes *Cryptosporidium parvum* solution (1×10^5 oocysts per mL) were injected respectively, the outflow was continuously collected. Fig. 4.1 shows the schematic description of the experiment.

NaCl - tap water solution is used as tracer, which experiences only advection and dispersion. The *Cryptosporidium parvum* can be classified as biological colloid. Colloids moving in porous media experience advection, dispersion, sorption-desorption, and filtration.

4.1.2 Analytical solution

For the one-dimensional transport including sorption-desorption and filtration through a homogeneous medium the following differential equation is applied

$$\frac{\partial C}{\partial t} + \frac{\rho_b}{n}\frac{\partial C_S}{\partial t} = v\alpha_L \frac{\partial^2 C}{\partial x^2} - v(\frac{\partial C}{\partial x} + \lambda C) \tag{4.1}$$

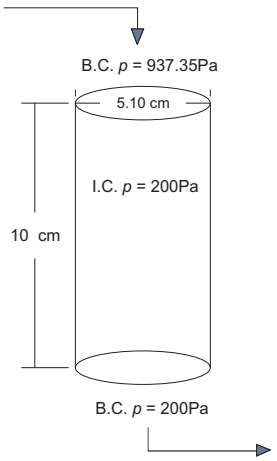

Figure 4.1: Schematic of soil column experiment

where C is dissolved concentration (kg·m^{-3}), C_S is sorbed concentration (kg·kg^{-1}), t is time (s), ρ_b is bulk density (kg·m^{-3}), n is porosity (-), v is velocity (m·s^{-1}), α_L is longitudinal dispersivity (m), x is distance (m), and λ is filtration coefficient (m^{-1}).

The instantaneous, linear sorption model assumes that

$$C_S = K_d C \tag{4.2}$$

where K_d is the partitioning coefficient ($m^3 \cdot kg^{-1}$). The retardation coefficient R is

$$R = 1 + \frac{\rho_b}{n} K_d \tag{4.3}$$

The dispersion coefficient in the x-direction D_{xx} ($m^2 \cdot s^{-1}$) is

$$D_{xx} = v\alpha_L \tag{4.4}$$

The analytical solution for a pulse input is (van Genuchten, 1981):

$$\begin{aligned} C = \ & \tfrac{1}{2} C_0 \Bigg[\exp\left(\frac{vx(1-\gamma)}{2D_{xx}}\right) \operatorname{erfc}\left(\frac{x - v\gamma t/R}{2\sqrt{D_{xx} t/R}}\right) \\ & + \exp\left(\frac{vx(1+\gamma)}{2D_{xx}}\right) \operatorname{erfc}\left(\frac{x + v\gamma t/R}{2\sqrt{D_{xx} t/R}}\right) \Bigg] \end{aligned} \tag{4.5}$$

for $t \in (0, \tau)$, (injection time from 0 to τ)

$$\begin{aligned} C = \ & \tfrac{1}{2}C_0\Bigg[\exp\left(\frac{vx(1-\gamma)}{2D_{xx}}\right)\operatorname{erfc}\left(\frac{x - v\gamma t/R}{2\sqrt{D_{xx}t/R}}\right) \\ & + \exp\left(\frac{vx(1+\gamma)}{2D_{xx}}\right)\operatorname{erfc}\left(\frac{x + v\gamma t/R}{2\sqrt{D_{xx}t/R}}\right) \\ & - \exp\left(\frac{vx(1-\gamma)}{2D_{xx}}\right)\operatorname{erfc}\left(\frac{x - v\gamma(t-\tau)/R}{2\sqrt{D_{xx}(t-\tau)/R}}\right) \\ & - \exp\left(\frac{vx(1+\gamma)}{2D_{xx}}\right)\operatorname{erfc}\left(\frac{x + v\gamma(t-\tau)/R}{2\sqrt{D_{xx}(t-\tau)/R}}\right)\Bigg] \end{aligned} \tag{4.6}$$

for $t \in (\tau, \infty)$, where

$$\gamma = \sqrt{1 + 4v\lambda R D_{xx}/v^2} \tag{4.7}$$

4.1.3 Numerical solution

The calculation area is simplified to a line with the length of 0.1m. For the numerical model 100 elements and 101 nodes are included. Head gradient is set by giving two constant pressures at both left and right boundaries to establish a uniform velocity field with the value of 7.1 md^{-1}.

The number of pore volume (x-axis) is calculated by

$$P_V = \frac{vt}{L} \tag{4.8}$$

where v is the seepage velocity, L is the length of the soil column. Considering the Courant number, the time step size is set by assigning P_V to 0.01. In the simulation, 100 particles per time steps are loaded near the left boundary for 250 time steps.

The filtration process is described by using the filtration coefficient. The sorption-desorption process is described by the two-rate model from Johnson et al. (1995). In the two-rate model, desorption is governed by two different rate coefficients

$$N/N_0 = Ae^{-k_1 t} + (1 - A)e^{-k_2 t} \tag{4.9}$$

where N is the number of particles remaining on the medium at time t, N_0 is the initial number of particles on the medium at the time of initial sorption, A is a weighting factor, and k_1 and k_2 are the fast and slow sorption rate coefficient, respectively. Relevant parameters are listed in Tab. 4.1.

Table 4.1: Model parameters for the column experiment

Symbol	Parameter	Value	Unit
k	Permeability	1.114476×10^{-11}	m^2
α_L	Longitudinal dispersivity	0.005	m
n	Porosity(tracer)	0.5	–
n	Porosity(colloid)	0.42	–
A	Weighting factor	0.9	–
k_1	Fast sorption rate coefficient	0.1	–
k_2	Slow sorption rate coefficient	0.001	–
λ	Filtration coefficient	5.2	m^{-1}

4.1.4 Results

The tracer experiences only advection and dispersion, which means in Eq. 4.1, $C_S = 0$, $\lambda = 0$. The results of RWPT simulation for the distribution of concentration over time are compared to those of measured value from the experiment by Harter, the analytical solution, and the OGS simulation with the mass transport method. The comparison results are shown in Fig. 4.2, where the green curve is the measured value, the dashed black curve is the simulation result operated with FEM, the blue curve is the RWPT simulation result, and the red curve is the analytical solution.

In the colloid transport simulation, the number of particles leaving the right boundary is counted each time step. The number is then converted to concentration in order to obtain the corresponding breakthrough curve over time. The comparison with the measured value

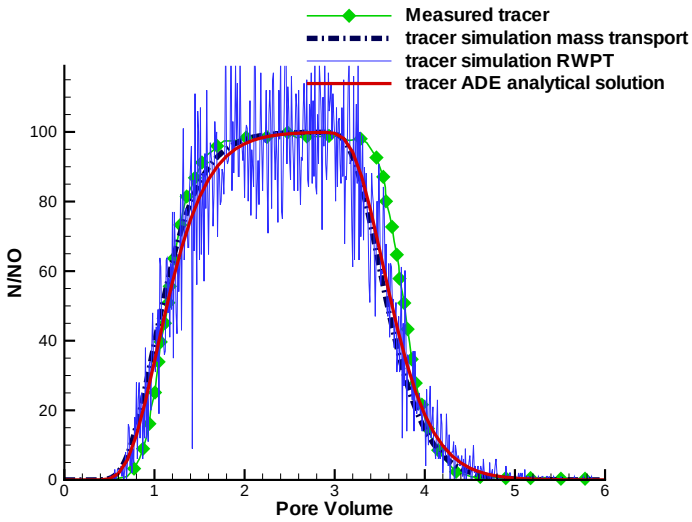

Figure 4.2: Tracer transport with advection and dispersion

from Harter's experiment is shown in Fig. 4.3, where the green curve is the measured value, and the blue curve is the RWPT simulation result. No analytical solution is available in this kind of situation.

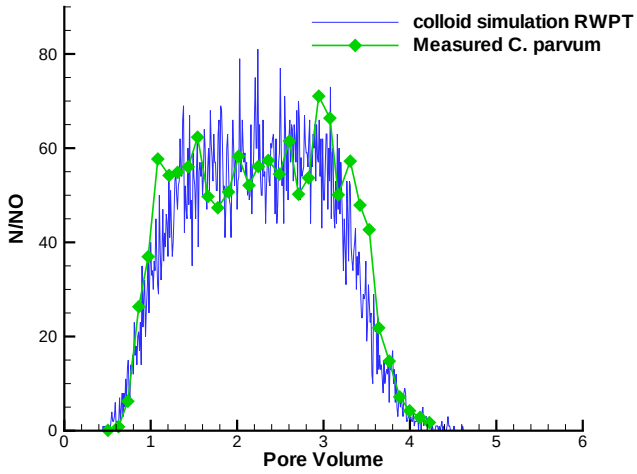

Figure 4.3: Colloid transport with sorption-desorption and decay

4.2 RWPT in homogeneous porous medium: 2D case study

4.2.1 Definition

A two-dimensional homogeneous aquifer is chosen to verify advective dispersive transport. The dimension of the model domain is 184 m by 64 m where the uniform velocity field is held constant in the x direction (Fig. 4.4).

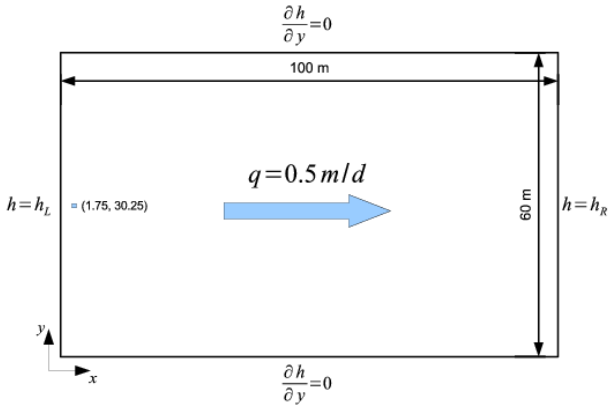

Figure 4.4: Schematic of 2D homogeneous model

4.2.2 Analytical solution

The stated problem can be solved with an analytical solution provided by Ogata and Banks (1961).

$$C\left(x,y,t\right)=\frac{C_0 A}{4\pi t\sqrt{D_{xx}+D_{yy}}}\exp\left[-\frac{\left(x-x_0\right)^2}{4D_{xx}t}-\frac{\left(y-y_0\right)^2}{4D_{yy}t}\right] \tag{4.10}$$

where C_0 is the initial concentration.

4.2.3 Numerical solution

The domain is discretized with quadrilateral elements of 0.5 m by 0.5 m. The same grid density is also used for converting particle distributions to element concentrations. The head gradient of one in the x direction is set by assigning two constant boundary conditions

along both the left and right sides, thus obtaining the uniform velocity field with the value of 0.5 md^{-1}.

The initial source load is applied to an area with dimensions of 0.1 m by 0.1 m to have an initial concentration of $C_0 = 1\ kgm^{-3}$. The material properties for this model setup are given in Tab. 4.2.

Table 4.2: Material properties for 2D homogeneous medium

Symbol	Parameter	Value	Unit
k	Permeability	1.114×10^{-11}	m^2
α_L	Longitudinal dispersivity	0.1	m
α_T	Transverse dispersivity	0.1	m

4.2.4 Results

Transport results of the RWPT method compared with the analytical solution at 20, 40, and 60 days are provided in Fig. 4.5. The solid line is the analytical solution, the dotted line is the RWPT result. Contour lines are shown for $C = 2.6e^{-4}$, $1.6e^{-4}$, $1.0e^{-4}$, and $4e^{-5}$. The number of particles used for this simulation is 50000. This is significantly less than the number of particles reported by Hassan and Mohamed (2003), who stated that up to 2.5 million particles were necessary to achieve smoothness of the solution due to oscillations around the contours. As the oscillations observed here for the method proposed are smaller than reported by Hassan and Mohamed (2003), the proposed method allows a dramatic reduction of around two orders of magnitude in the number of particles required for a smooth solution.

In addition, different numbers of particles are used to solve the same problem, producing several different particle clouds as shown in Fig. 4.6. Fig.(a-d) show the particle clouds of 50000 particles at 0, 20, 40, and 60 days, Fig.(e) shows particle clouds of 1000, 5000, 10000, and 50000 particles at 60 days.

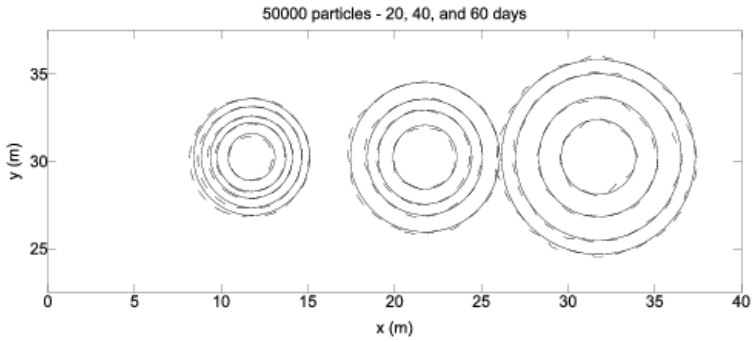

Figure 4.5: Transport results of the 2D RWPT method compared with analytical solution

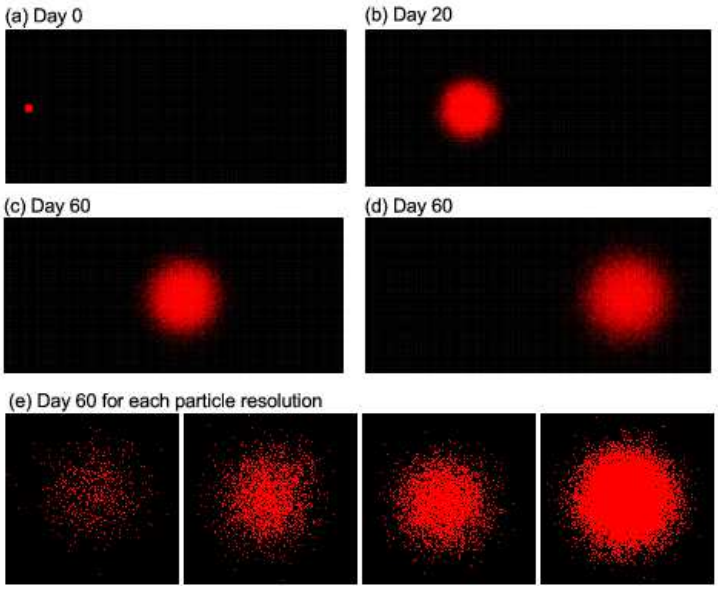

Figure 4.6: Particle clouds at different days

4.3 RWPT in 2D homogeneous porous medium with sorption and decay

The model in section 4.2 only considers the process of advection and dispersion. In this section, the process of sorption and decay are involved respectively and can be compared with the results presented in section 4.2.

Use the same calculation domain and boundary conditions as section 4.2, keep all the parameters unchanged and add the sorption process. Two-rate sorption model which is mentioned in section 4.1 is adopted here with A=0.5, $k1$=0.1,$k2$=0.0001. The simulation result of particle distribution over time is shown in Fig. 4.7. Particles are absorbed randomly at every time step according to the two-rate sorption model. The absorbed particles appear to hesitate at their movement. As the desorption process exists, absorbed particles still have the chance to move again. Thus the particle cloud is not a circle any more. The absorbed particles change the shape of the cloud which makes the distribution more widely spread. Note that the colors of the particles represent for the mobility of particles that free particles are colored in blue, and absorbed particles are gray.

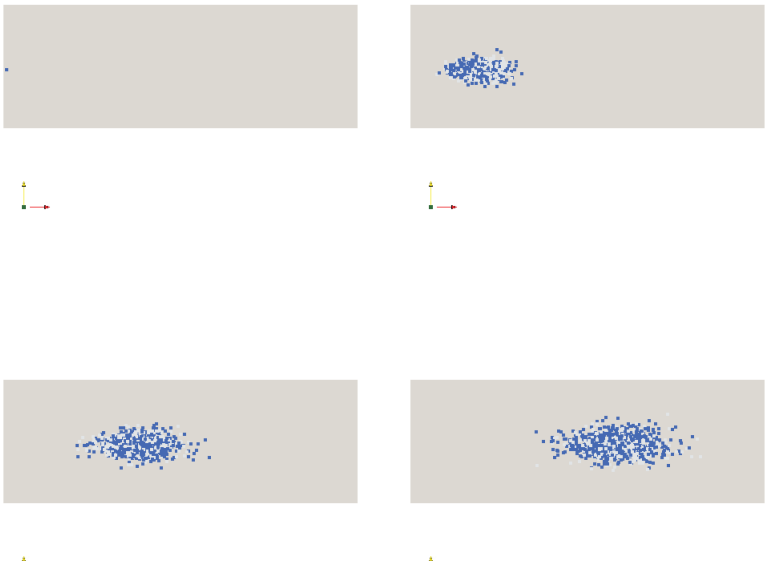

Figure 4.7: Particle clouds in 2D homogeneous media with sorption

Use the same calculation domain and boundary conditions as section 4.2, keep all the parameters unchanged and add the decay process. First-order kinetic decay which is mentioned in section 4.1 is adopted with λ=5e-3. The simulation result of particle distribution over time is shown in Fig. 4.8. Particles decay randomly at every time step according to the first-order kinetic decay model. Decayed particles terminate their movement permanently. The particle cloud consists of a main circle and a long tail behind, which is composed by the decayed particles. Note that the colors of the particles represent for the mobility of particles that free particles are colored in blue, absorbed particles are gray, and decayed particles are red.

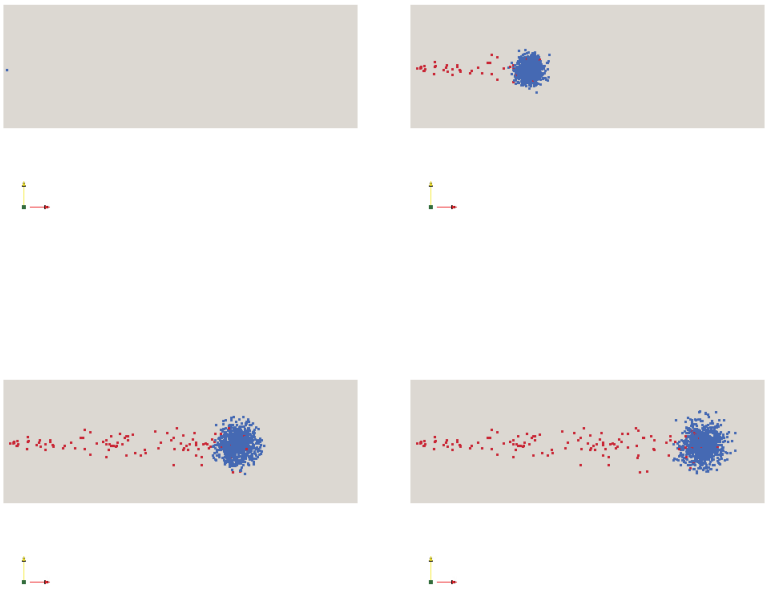

Figure 4.8: Particle clouds in 2D homogeneous media with decay

4.4 RWPT in heterogeneous porous medium: 2D case study

4.4.1 Definition

A two-dimensional heterogeneous aquifer is chosen to verify advective dispersive transport. The dimension of the model domain is 184 m by 64 m.

4.4.2 Numerical solution

The domain is discretized with quadrilateral elements of 0.5 m by 0.5 m. The same grid density is also used for converting particle distributions to element concentrations. The head gradient of one in the x direction is set by assigning two constant boundary conditions along both left and right sides.

The initial source load is applied to an area with dimensions of 0.1 m by 0.1 m to have an initial concentration of $C_0 = 1\ kgm^{-3}$. The material properties for this model setup are given in Tab. 4.3.

Table 4.3: Material properties for 2D heterogeneous medium

Symbol	Parameter	Value	Unit
α_L	Longitudinal dispersivity	0.1	m
α_T	Transverse dispersivity	0.1	m

The permeability of this domain is with randomly distributed value at different positions. The distribution of the permeability is shown in Fig. 4.9.

4.4.3 Results

Dirichlet boundary conditions are adopted that constant hydraulic heads are set on both left and right sides. The distribution of the pressure is shown in Fig. 4.10. The equipotential lines are not exactly parallel to each other but the tendency are the same, because the geometry of the model is relatively simple.

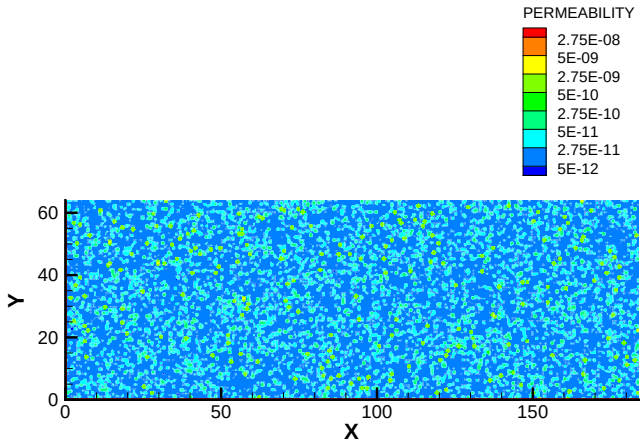

Figure 4.9: Distribution of the permeability in 2D heterogeneous media

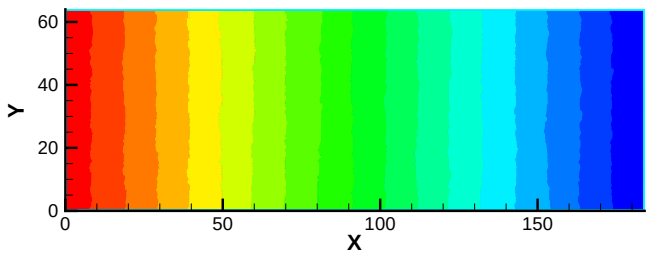

Figure 4.10: Distribution of the pressure in 2D heterogeneous media

The simulation result of particle distribution over time is shown in Fig. 4.11. Comparing to Fig. 4.6, the shape of the clouds are similar but their positions at different times are different from each other. Apparently this is caused by the difference of flow field properties in these two models, as the movements of particles only take use of the velocity distribution. This benchmark shows the capability of the proposed RWPT method to be used in aquifers with heterogeneity.

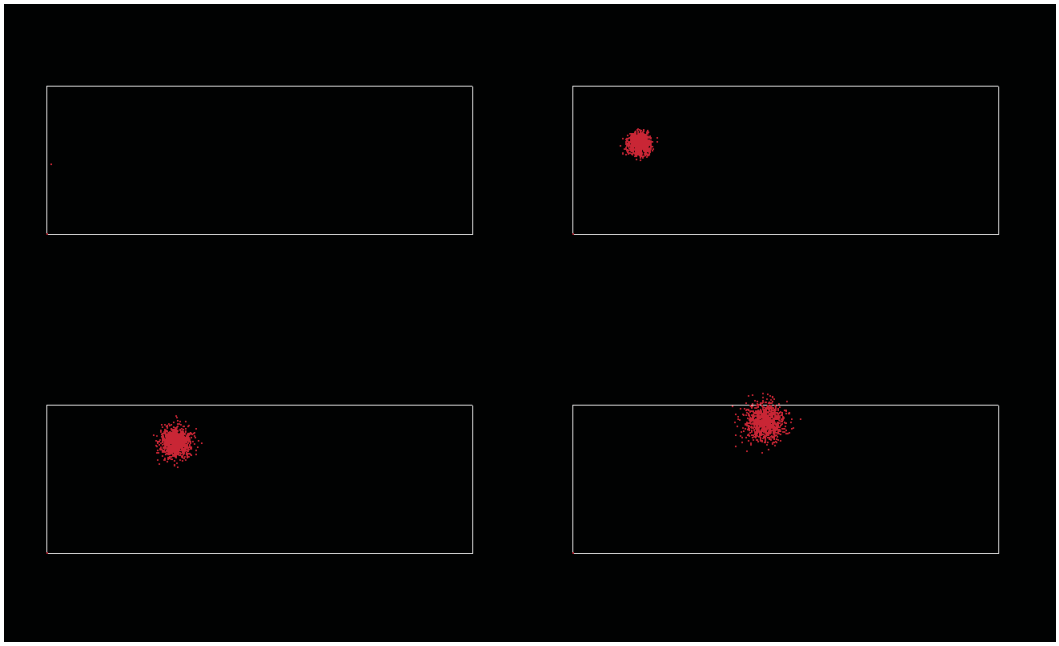

Figure 4.11: Particle Clouds in 2D heterogeneous media

4.5 RWPT in homogeneous porous medium: 3D case study

4.5.1 Definition

A three-dimensional homogeneous cube is chosen to verify advective dispersive transport. The side length of the cube model domain is 100 m. The velocity field is held constant in the diagonal direction from the bottom left to top right (Fig. 4.12).

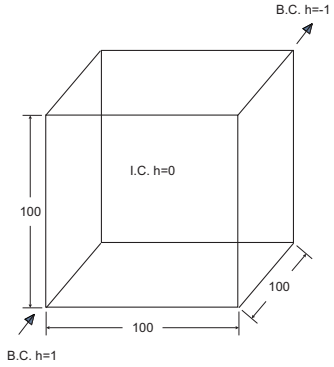

Figure 4.12: Schematic of 3D homogeneous model

4.5.2 Analytical solution

The stated problem can be solved with an analytical solution provided by Ogata and Banks (1961).

$$C\left(x,y,z,t\right)=\frac{C_0\mathbf{v}}{8\left(\pi t\right)^{3/2}\sqrt{D_{xx}D_{yy}D_{zz}}}\exp\left[-\frac{\left(x-x_0\right)^2}{4D_{xx}t}-\frac{\left(y-y_0\right)^2}{4D_{yy}t}-\frac{\left(z-z_0\right)^2}{4D_{zz}t}\right] \tag{4.11}$$

where C_0 is the initial concentration.

4.5.3 Numerical solution

The domain is discretized with tetrahedral elements. The same grid density is used for converting particle distributions to element concentrations. The head gradient is set by assigning two constant boundary conditions on the diagonal joint points.

The initial source load is applied to an area close to the bottom left of the domain with an initial concentration of $C_0 = 1\ kgm^{-3}$. The material properties for this model setup are given in Tab. 4.4.

4.5.4 Results

The advection-dispersion of the particles pulse across the cube is shown in Fig. 4.13. At the beginning, particles are assembled together as they were released from positions

Table 4.4: Material properties for 3D homogeneous medium

Symbol	Parameter	Value	Unit
k	Permeability	6.0804×10^{-10}	m^2
α_L	Longitudinal dispersivity	0.005	m
α_T	Transverse dispersivity	0.005	m
n	Porosity	0.2	–

that are very close to each other. As the particles moving along with the flow, they disperse and form a spherical surface-shaped cloud. When the particles move to the center of the cube, the area of the spherical surface-shaped cloud reach to the maximum. After particles across the center of the cube, as the flowpaths begin to converge, the shape of the particle cloud change to a funnel-shaped curved surface. Particles move along the diagonal line have the bigger velocities and shorter pathlines so they reach to the top right corner of the cube earlier than other particles.

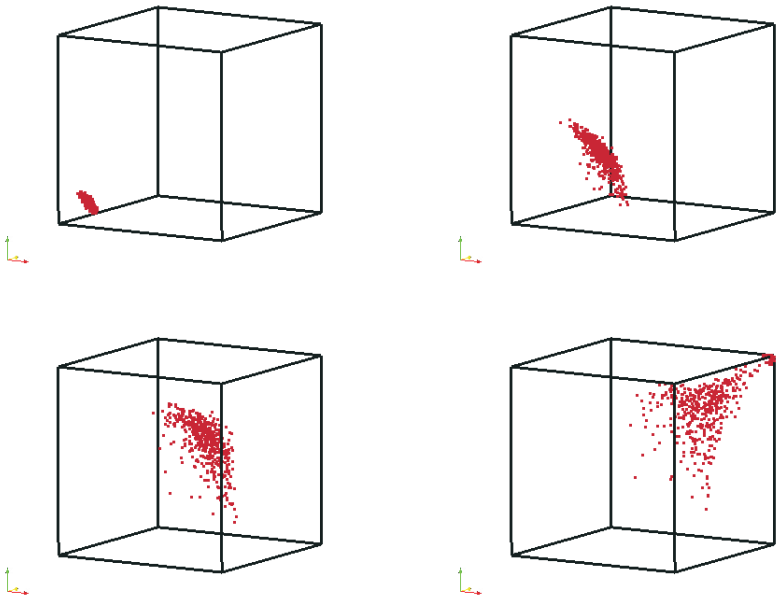

Figure 4.13: Particle clouds in the cube

The number of particles that pass the top right corner of the cube is counted at every time step in order to generate the concentration breakthrough curve. The result of RWPT simulation for the distribution of concentration over time is compared to the analytical solution. The comparison results are shown in Fig. 4.14, where the blue curve is the RWPT simulation result, and the red curve is the analytical solution. The shape of the breakthrough curve is classical and similar to 1D and 2D simulations. With a relatively large number of particles the problem of fluctuations in concentration calculation can be overcome.

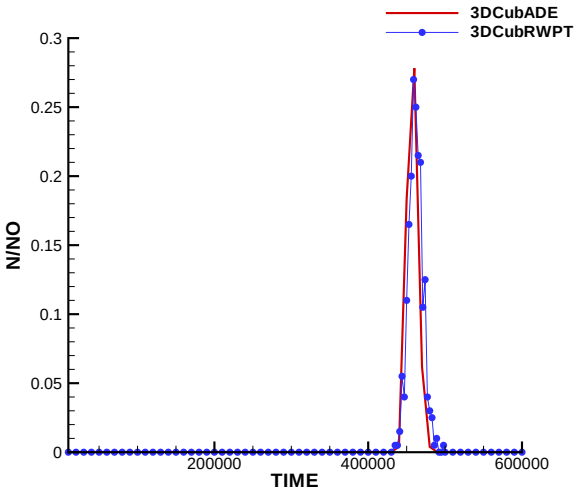

Figure 4.14: Transport results of the 3D RWPT method compared with analytical solution

This benchmark shows that the proposed RWPT method can describe the fluid flow and solute transport in more details comparing to the traditional finite element method. With the post-processing programming one can observe the visualized results of the movement of every single particle at any time step, and the development of the particle cloud over time. While with the traditional finite element method one can only get the result of concentration distribution.

4.6 RWPT in pore scale: 2D case study

Physical observations and theoretical treatments of flow in porous media are usually associated with three different length scales: pore-, local-, and field-scales. Dominant processed and governing equations may vary with scales. In this benchmark, efforts are taken in order to simulate solute transport in pore scale in a simplified manner. The governing equation adopted here is the groundwater flow equation based on Darcy's law.

4.6.1 Definition

To simulate particles moving in pore scale space, first the problem is simplified into a two-dimensional case which is a box with only one grain inside. The calculation area is a rectangular space with a circle in the middle, the void between the circle and the rectangular is the calculation domain and discretized by triangle mesh (Fig. 4.15).

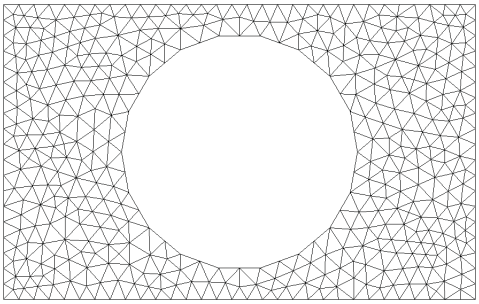

Figure 4.15: Mesh of 2D box with one grain inside

4.6.2 Numerical solution

Firstly, the proposed RWPT method in this model is testified by assign constant hydraulic head to the left and right boundaries (Dirichlet boundary condition), and no-flow boundary conditions to the top and bottom boundaries. Particles are released from a line that is close to the left boundary. Relative parameters are listed in Tab. 4.5.

Table 4.5: Material properties for 2D pore scale model with one grain inside - advective

Symbol	Parameter	Value	Unit
k	Permeability	1×10^{-10}	m^2
D_d	Diffusion coefficient	0.0	$\mathrm{m}^2\mathrm{s}^{-1}$
n	Porosity	1.0	$-$

4.6.3 Results

The particles are moving in the pore space according to the velocity field. Particle cloud develops over time is show in Fig. 4.16.The shape of the particle cloud is a straight line in the beginning, and then is curved a little as it getting closer to the grain. The velocities in the area surrounding the grain are very small that particles in this area are moving very slowly. When a particle hit the surface of the grain or the boundary of the box, it will be captured. Particles pass through the throats between the grain and the box are accelerated as the velocities in these throats are large. After passing through the throats, particles spread to form an arc and move on to the right side boundary. In the zone that is behind the grain no particles are observed because the flow velocity is relatively small and dispersion is not considered in this benchmark.

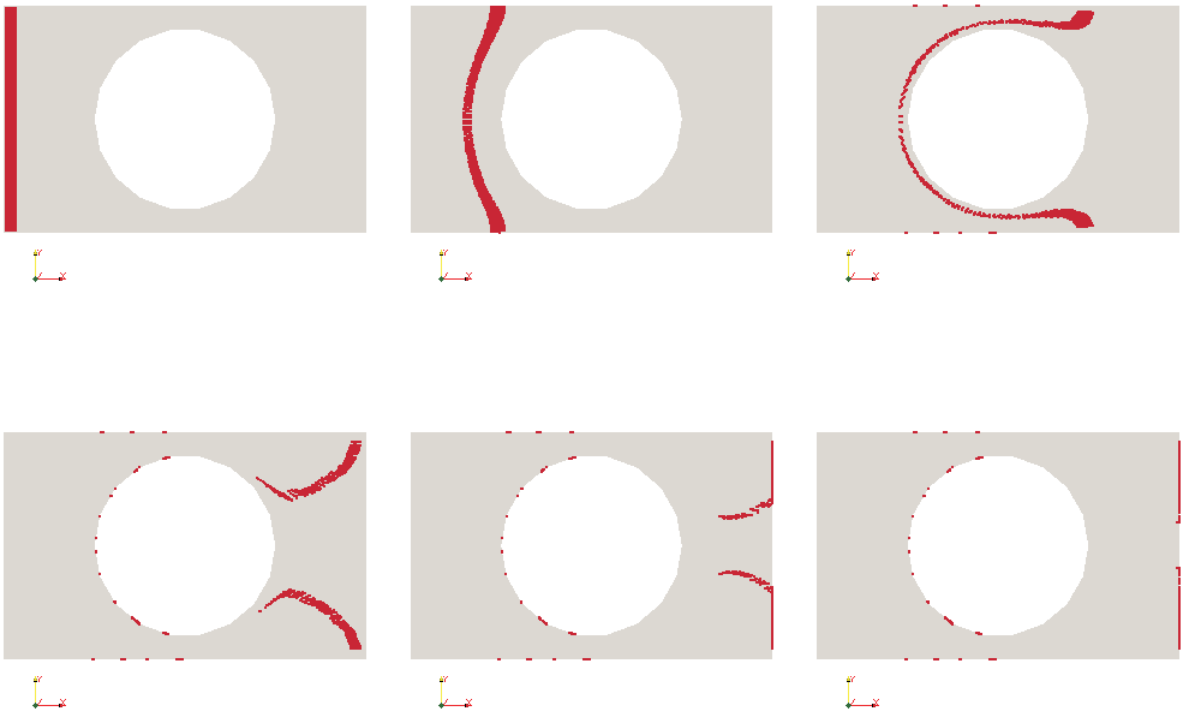

Figure 4.16: Particles advect in rectangular domain with one grain

4.6.4 Discussion 1

If there is no flow in this domain, and the molecular diffusion coefficient is increased, then the movements of the particles are dominated by the molecular diffusion process. Relative parameters are listed in Tab. 4.6.

Table 4.6: Material properties for 2D pore scale model with one grain inside - diffusive

Symbol	Parameter	Value	Unit
k	Permeability	1×10^{-10}	m^2
D_d	Diffusion coefficient	1×10^{-8}	$\mathrm{m}^2\mathrm{s}^{-1}$
n	Porosity	1.0	$-$

Particles are released from a line that is close to the left boundary. As there is no flow, particles are moving randomly in the pore space. Particle cloud develops over time is show in Fig. 4.17. Some of the particles attach to the surface of the grain or the boundary of the box. The molecular diffusion coefficient is relative to temperature. This benchmark is aimed to achieve the effect that particles are moving differently when temperature changes.

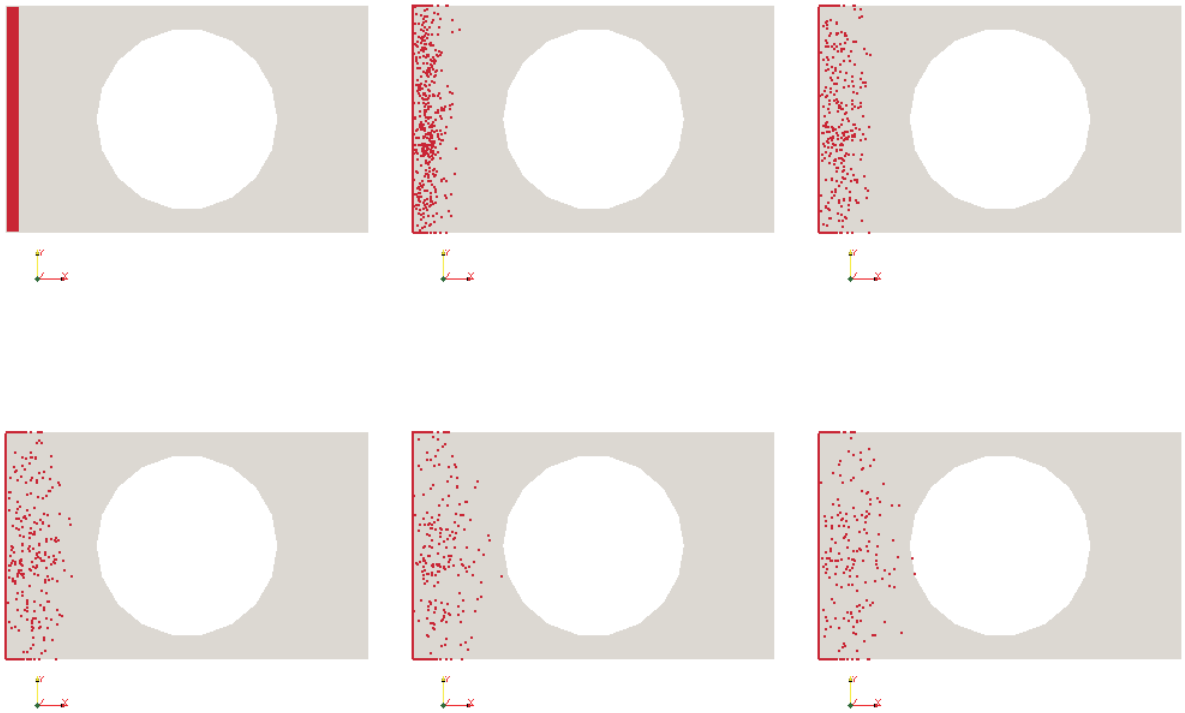

Figure 4.17: Particles diffuse in rectangular domain with one grain

4.6.5 Discussion 2

Next, the number of grains in the box is increased from one to six. The void between the circles and the rectangular is the calculation domain and discretized by triangle mesh (Fig. 4.18). Dirichlet boundary conditions are set by assign constant hydraulic head to the left and right boundaries. No-flow boundary conditions are set to the top and bottom boundaries. Particles are released from a line that is close to the left boundary. Relative parameters are unchanged as listed in Tab. 4.5.

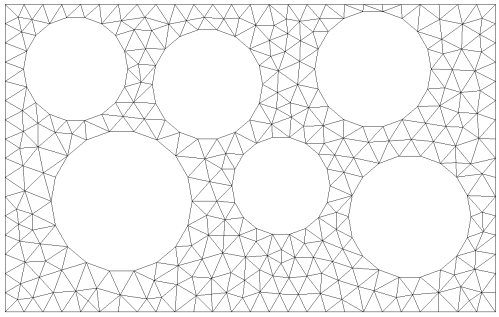

Figure 4.18: Mesh of 2D box with several grains inside

Particle cloud develops over time is show in Fig. 4.19. Note that in this benchmark, released particles are displayed in the color of blue. When a particle hits the boundary and gets attached, it turns to red. But in the next time step, the attached particle still has the chance to detach and move again. It is clear that this benchmark is not a simple combination of six single grains, because they can affect each other. The velocity field in this case is with more complexity thus the particle cloud is complicated. But the particle cloud development obeys the same trend as in the single grain case.

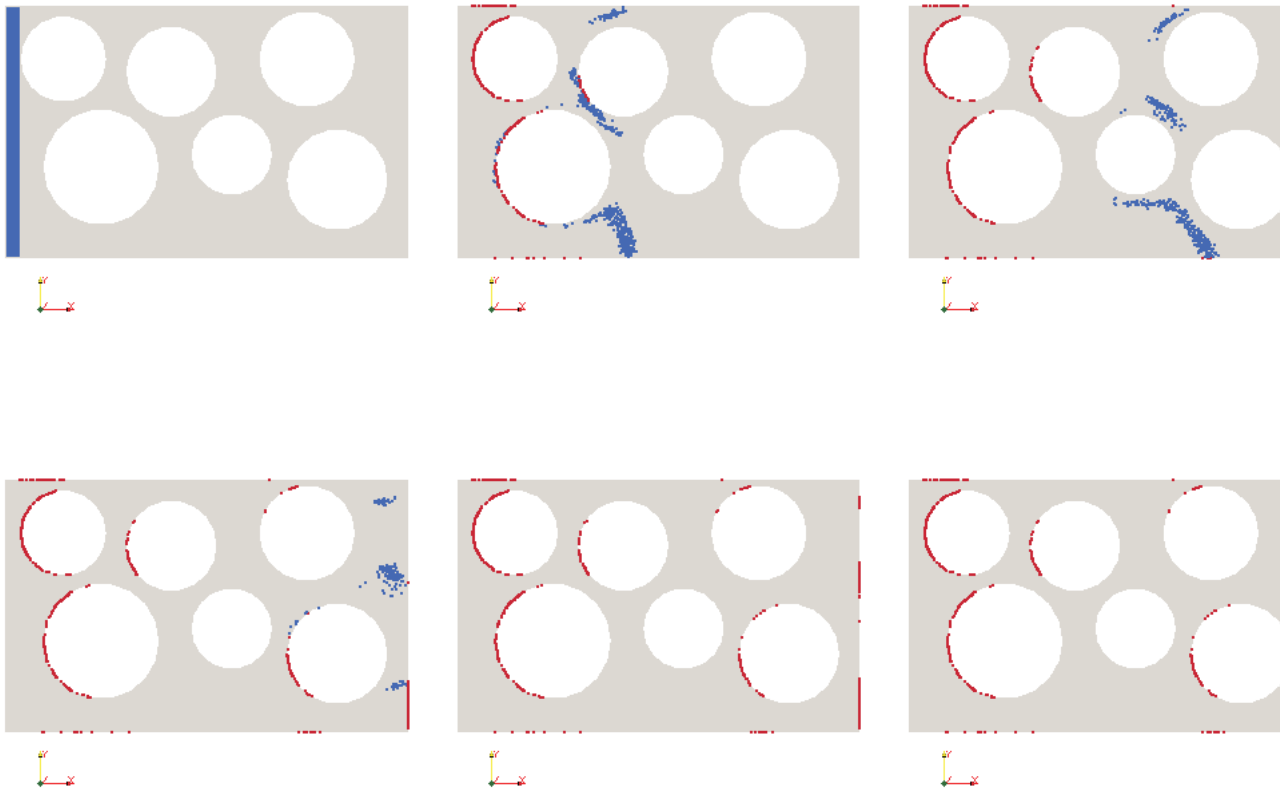

Figure 4.19: Particles transport in rectangular domain with several grains

4.6.6 Discussion 3

If the grain (circle) is discretized inside (Fig. 4.20), then particles attached to the surface of the grain can go into the grain and diffuse inside. Different porosity and permeability coefficient are given to grains and the pore space. Note that the different colors here represent materials with different properties. Dirichlet boundary conditions are set by assign constant hydraulic head to the left and right boundaries. No-flow boundary conditions are set to the top and bottom boundaries. Particles are released from a line that is close to the left boundary. Relative parameters are listed in Tab. 4.7.

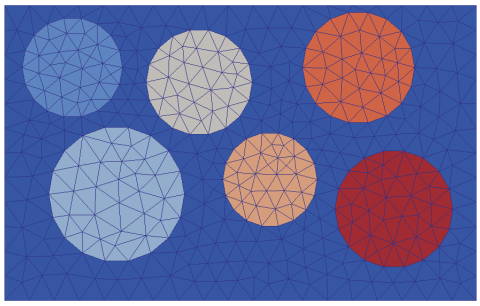

Figure 4.20: Mesh of 2D box with meshed grains inside

Table 4.7: Material properties for 2D pore scale model with six meshed grains inside

Symbol	Parameter	Value	Unit
k	Permeability (pore space)	1×10^{-10}	m^2
k	Permeability (grains)	1×10^{-12}	m^2
D_d	Diffusion coefficient	1×10^{-15}	m^2s^{-1}
n	Porosity (pore space)	1.0	–
n	Porosity (grains)	0.1	–

Particle cloud develops over time is show in Fig. 4.21. The particles in the pore space are moving according to the velocity field. Note that there's no flow inside of the grains, only molecular diffusion. Particles that hit the surface of the grains can go into the grains

and move inside. Their movements are because of molecular diffusion thus are random.

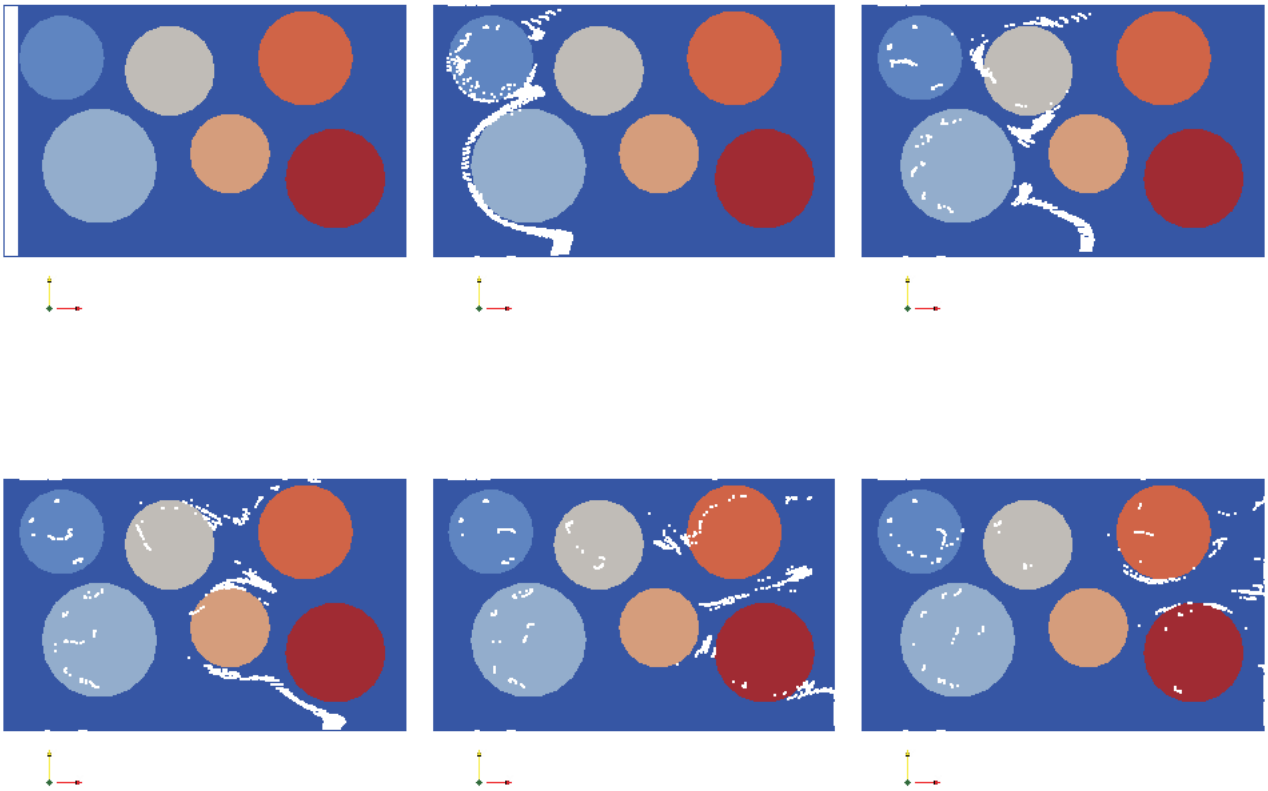

Figure 4.21: Particles transport in rectangular domain with several meshed grains

4.7 RWPT in pore scale: 3D case study

4.7.1 Definition

Similar to the 2D case study, the problem is first simplified into a three-dimensional case with only one grain in a box. The calculation area is a cube space with a sphere in the center, the void space between the sphere and the cube is the calculation domain and discretized by tetrahedral mesh (Fig. 4.22).

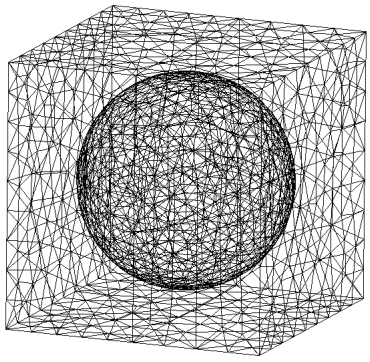

Figure 4.22: Mesh of 3D box with one grain inside

4.7.2 Numerical solution

The proposed RWPT method in this model is testified by assign constant hydraulic head to the left surface and right surface boundaries (Dirichlet boundary condition), and no-flow boundary conditions to the top, bottom, front, and back surface boundaries. Particles are released from a surface that is close and parallel to the left surface boundary. Relative parameters are listed in Tab. 4.8.

4.7.3 Results

The particles are moving in the pore space according to the velocity field. Particle cloud develops over time is show in Fig. 4.23. The shape of the particle cloud is a plain surface

Table 4.8: Material properties for 3D pore scale model with one grain inside

Symbol	Parameter	Value	Unit
k	Permeability	1×10^{-10}	m^2
D	Diffusion coefficient	1×10^{-15}	m^2s^{-1}
n	Porosity	1.0	$-$

in the beginning, then is curved a little as it getting closer to the grain. The velocities in the area surrounding the grain is very small that particles in this area are moving very slowly. When a particle hit the surface of the grain or the box, it will be attached. In the zone that is behind the grain no particles are observed because the flow velocity is relatively small that no turbulence is happened in that zone.

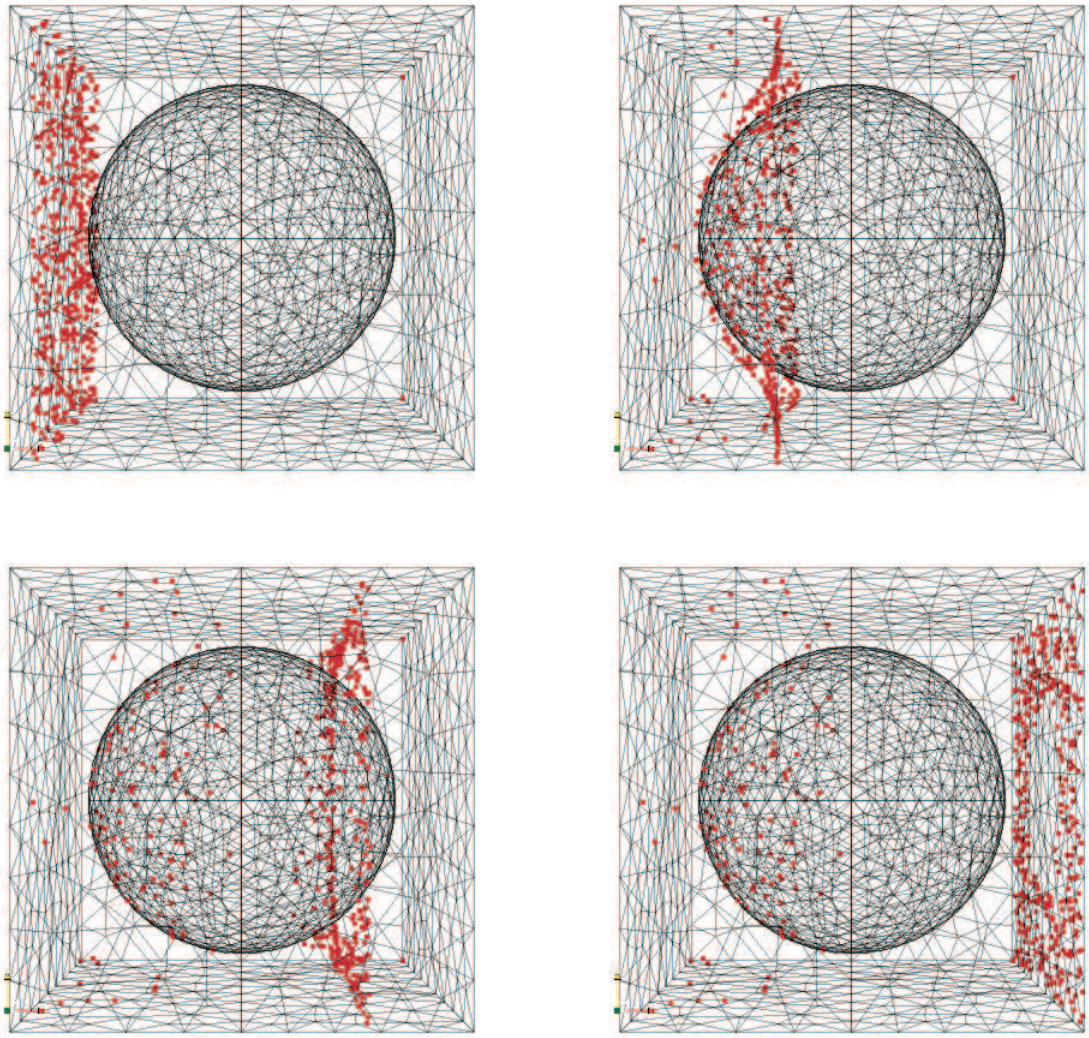

Figure 4.23: Particles advect in cube domain with one grain

Chapter 5

Flow processes

The accuracy of the velocity field calculation is crucial to the precision of the RWPT method. In groundwater flow simulation, the velocity field is determined by the hydraulic head or pressure difference according to Darcy's law. However, when the velocity is higher, inertial effects can be significant and need for consideration; the non-linear impact of the pressure difference to the velocity can be described by Forchheimer flow. Another consideration in groundwater simulation is the saturation of the soil, if the soil is unsaturated, for example in the vadose zone, Richards flow is considered to describe the water movement. The proposed RWPT method is capable to be adopted with different flow processes since the displacements of the particles are calculated according to the velocity field, regardless of how it is obtained.

5.1 Forchheimer flow

5.1.1 Forchheimer term

Modeling groundwater flow in porous media typically makes use of Darcy's law and equation of mass conservation to establish the groundwater flow equation, as discussed in section 2.1. For low velocity flows, Darcy's law gives a good description of the flows and thus a number of linear forms have been developed (Dullien and Azzam, 1973; Whitaker, 1969). However, there are circumstances when the velocities are high that discrepancies

occur between the experimental observations and simulation results obtained according to Darcy's law.

Forchheimer flow describes the non-linear form of fluid flow in porous media in a scale that is smaller than the macro-scale domain size and larger than the micro-scale pore size. It is an extension of the Darcy's law when the viscous forces do not prevail over the inertial forces. A kinetic effect is considered and expressed as an additive term in the description of pressure difference. The classic form of Forchheimer term is written as (Forchheimer, 1901)

$$-\nabla P = \frac{\mu}{k}\mathbf{q} + \beta\rho|\mathbf{q}|\mathbf{q} \tag{5.1}$$

where $\mu[MT^{-1}L^{-1}]$ is the dynamic viscosity of water, $k[L^2]$ is intrinsic permeability, $\mathbf{q}[LT^{-1}]$ is Forchheimer velocity vector, $\beta[L^{-1}]$ is Forchheimer coefficient, and $\rho[ML^{-3}]$ is density of water.

The Forchheimer coefficient β is also known as non-Darcy coefficient. Several approaches have been applied to obtain the value of β (Balhoff et al., 2010; Chilton and Colburn, 1931; Ergun and Orning, 1949). The formulae are normally defined for certain flow conditions. There is no general agreement on the nature of this coefficient. Some of the approaches are based on empirical results and some on fundamental characterizations of the porous media. Parameters involved in the calculation of β include permeability, as well as porosity, and tortuosity in some cases.

5.1.2 Forchheimer flow in 1D porous medium

The 1D homogeneous porous medium benchmark (see section 4.1 for description) is adopted in order to compare different behaviors of flow under Darcy and Forchheimer regimes, and their influence on solute transport performance which is simulated with particle tracking.

Governing equations

If we consider the hydraulic head $h = \frac{P}{\rho g} + z$, where $z[L]$ is elevation head, and neglect the gravitational effect, then the Forchheimer equation (5.1) can be written as

$$-\nabla h = \frac{1}{K}\mathbf{q} + \frac{\beta}{g}|\mathbf{q}|\mathbf{q} \tag{5.2}$$

where K $[LT^{-1}]$ is hydraulic conductivity and $K = \frac{k\rho g}{\mu}$. In the OGS simulation of Forchheimer flow, $\frac{1}{K}$ is referred to as a_1 and $\frac{\beta}{g}$ as a_2, and they are used as coefficients for the calculation.

$$-\nabla h = a_1\mathbf{q} + a_2|\mathbf{q}|\mathbf{q} \tag{5.3}$$

The equation of mass conservation that describes the groundwater flow without source term can be formed as

$$-\nabla \mathbf{q} = S_s\frac{\partial h}{\partial t} \tag{5.4}$$

where S_s $[L^{-1}]$ is the storativity (volumetric specific storage), t $[T]$ is time.

In 1D case, equation (5.3) and equation (5.4) can be rewritten as

$$-\frac{\partial h}{\partial x} = a_1 q + a_2 q^2 \tag{5.5}$$

$$S_s\frac{\partial h}{\partial t} + \frac{\partial q}{\partial x} = 0 \tag{5.6}$$

Steady state flow with Dirichlet boundary condition

For the steady state flow, constant hydraulic heads are set at the inlet and outlet boundaries. Relevant parameters for the flow are listed in Tab. 5.1.

Forchheimer velocity can be calculated from equation (5.5) that

$$q = \frac{-a_1 + \sqrt{{a_1}^2 - 4a_2\frac{\partial h}{\partial x}}}{2a_2} \tag{5.7}$$

Darcy velocity can be obtained from equation (5.5) by assign $a_2 = 0$.

Simulation results of hydraulic head distribution and the comparison of Forchheimer velocity and Darcy velocity are shown in Fig. 5.1.

Table 5.1: Model parameters for the column experiment - steady state flow

Symbol	Parameter	Value	Unit
h_{in}	Hydraulic head(inlet)	0.09555	m
h_{out}	Hydraulic head(outlet)	0.02038	m
L	Column length	0.1	m
k	Intrinsic Permeability	1.114476×10^{-11}	m^2
K	Hydraulic conductivity	1.0933×10^{-4}	ms^{-1}
S_s	Volumetric specific storage	0.5	m^{-1}
a_1	OGS coefficient (equals to K^{-1})	9.146612×10^{3}	$m^{-1}s$
a_2	OGS coefficient	10^8	$m^{-2}s^2$

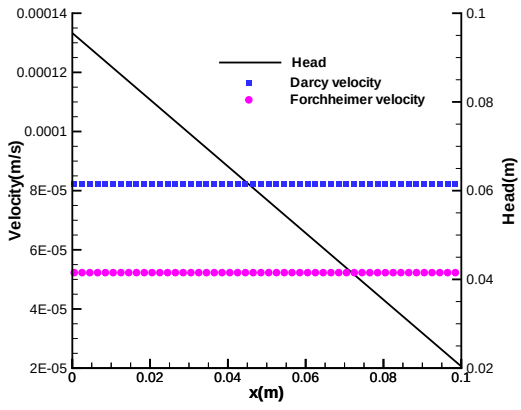

Figure 5.1: Forchheimer velocity and Darcy velocity in 1D steady state flow

The proposed RWPT method makes use of the velocities obtained from the flow process, regardless of the flow regimes. 25000 particles are injected at the inlet boundary for 2.5 pore volume ($P_V = vt/L$, $v = q/n$) to simulate non-reactive solute transport with slug input in 1D steady state flow under Forchheimer and Darcy regimes respectively. Parameters for the simulation of solute transport are listed in Tab. 5.2. Note that particles experience not only advection and hydrodynamic dispersion, but decay and retardation processes as well in this case. Detailed description for these processes is referred to in section 4.1.

Table 5.2: Model parameters for the column experiment - solute transport

Symbol	Parameter	Value	Unit
α_L	Longitudinal dispersivity	0.005	m
n	Porosity	0.42	–
A	Weighting factor	0.9	–
k_1	Fast sorption rate coefficient	0.1	–
k_2	Slow sorption rate coefficient	0.001	–
λ	Filtration coefficient	5.2	m^{-1}

Fig. 5.2 shows the simulation result of concentration breakthrough curve at $x = 0.1m$. Note that in RWPT method, the concentration is represented by the number of particles.

Transient flow with Dirichlet boundary condition

For unsteady, nonlinear flow in the 1D homogeneous porous medium, the same parameters are used as listed in Tab. 5.1. Simulation results of hydraulic head and velocity distributions under Forchheimer and Darcy regimes at $t = 5.1s$, $10.2s$, $15.3s$, $20.4s$, $25.5s$, $30.6s$ are shown in Fig. 5.4.

Particles are injected at the inlet boundary for 2.5 pore volume ($P_V = vt/L$, $v = q/n$) to simulate non-reactive advective-dispersive solute transport with slug input in 1D transient flow under Forchheimer and Darcy regimes respectively. Fig. 5.3 shows the simulation result of concentration breakthrough curve at $x = 0.1m$. Note that in RWPT method, the concentration is represented by the number of particles.

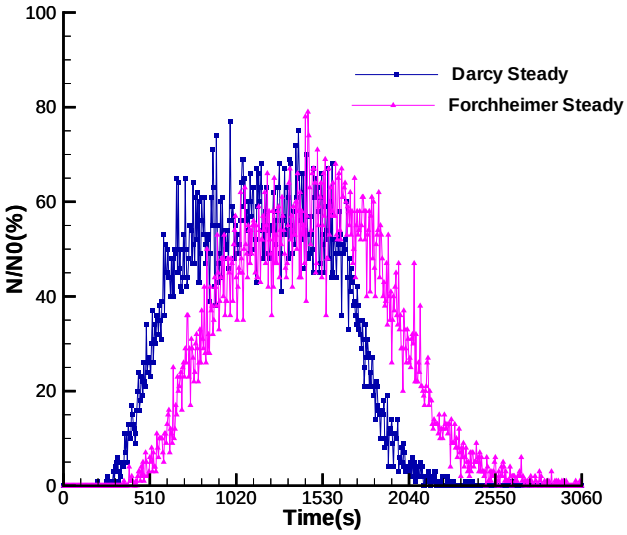

Figure 5.2: Particle tracking under Forchheimer and Darcy regimes in 1D steady state flow

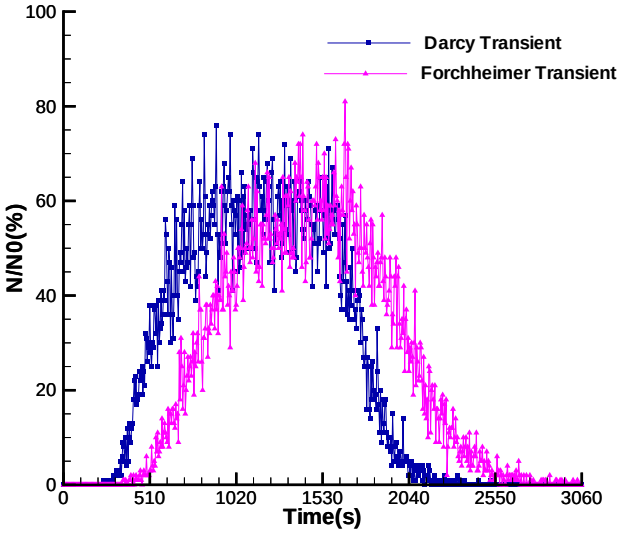

Figure 5.3: Particle tracking under Forchheimer and Darcy regimes in 1D transient flow

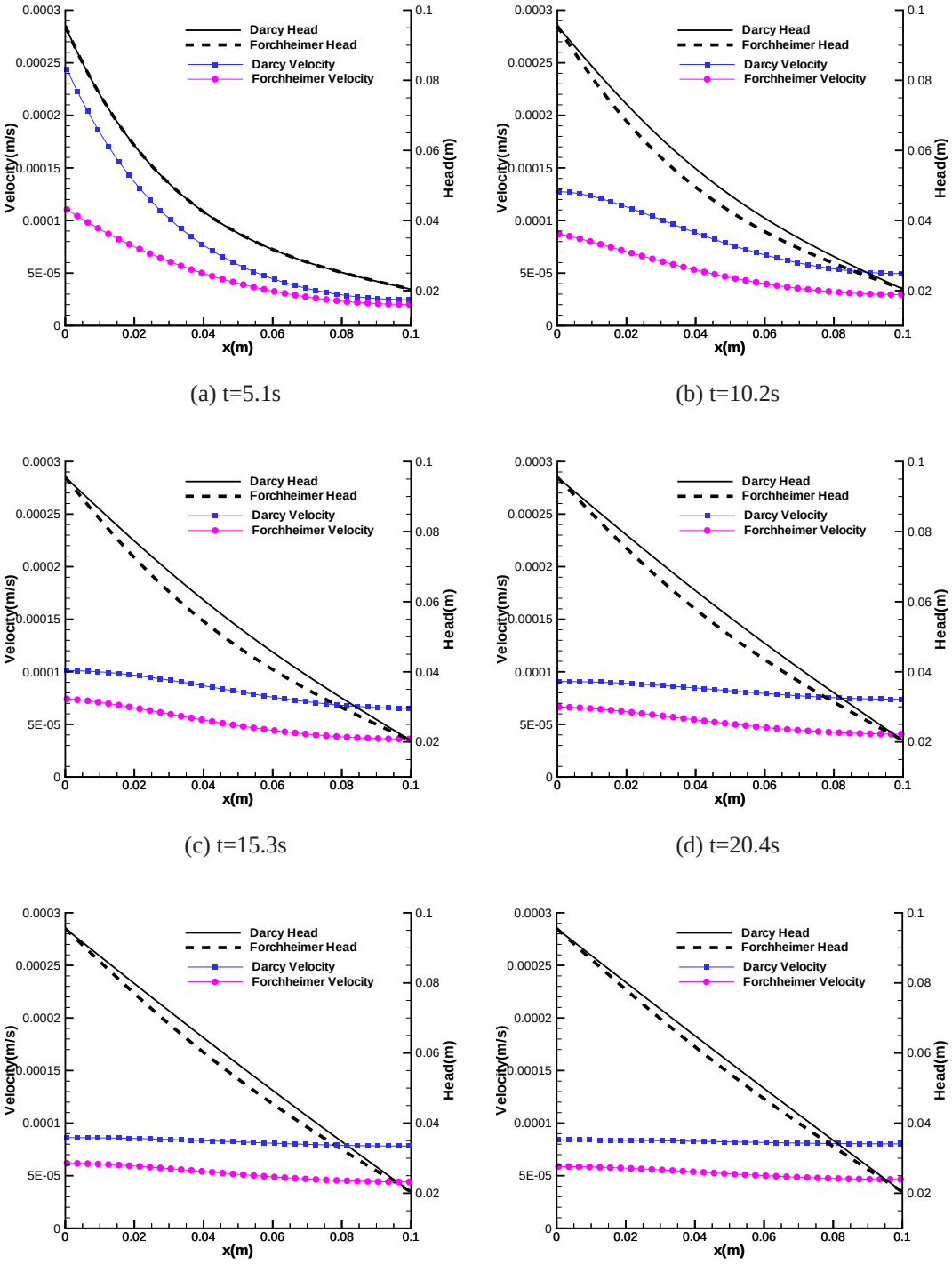

(a) t=5.1s (b) t=10.2s

(c) t=15.3s (d) t=20.4s

(e) t=25.5s (f) t=30.6s

Figure 5.4: Forchheimer velocity and Darcy velocity in 1D transient flow

5.1.3 Groundwater flow regimes

The applicability limits of Darcy's and Forchheimer's regimes of flow are of great interest. Ruth and Ma (1992) rearranged the Forchheimer equation (5.1) in the form

$$-\nabla P = \frac{\mu}{k}\mathbf{q} + \beta\rho|\mathbf{q}|\mathbf{q} = \frac{1}{k}(1 + \frac{\beta k\rho\mathbf{q}}{\mu})\mu\mathbf{q} = \frac{1}{k}(1 + F_o)\mu\mathbf{q} = \frac{\mu}{k_v}\mathbf{q} \tag{5.8}$$

and named $F_o[-]$ as Forchheimer number, and $k_v[L^2]$ as the velocity-dependent permeability. The Forchheimer number can be used as a criterion to indicate when the inertial force can prevail over the viscosity force. The velocity-dependent permeability shows that permeability can be treated as a velocity dependent parameter.

Apart from the Forchheimer number, another basic criterion to distinguish between these two regimes is the range of Reynolds number (Re), which is defined as the ratio of inertial forces to viscous forces and can be written as

$$Re = \frac{\rho\mathbf{q}L}{\mu} \tag{5.9}$$

where $\rho[ML^{-3}]$ is the density of water, $\mathbf{q}[LT^{-1}]$ is the specific discharge, $L[L]$ is the characteristic linear dimension, and $\mu[MT^{-1}L^{-1}]$ is the dynamic viscosity of water.

Darcy flow occurs at low Reynolds number, which means the dominant force in this situation is viscous force and the flow is comparatively smooth. In Forchheimer flow the inertial force prevails over the viscous force so the Reynolds number is high. The upper limit of Reynolds number in Darcy flow is considered to be coincided with the lower limit of Reynolds number in Forchheimer flow (Chilton and Colburn, 1931; Ergun, 1952; Fancher and Lewis, 1933; Green and Duwez, 1951; Hassanizadeh and Gray, 1987).

5.2 Richards flow

5.2.1 Richards equation

In the vadose zone, the soil is unsaturated that there are two phases of fluid, i.e. air and water, flow in the porous medium. The Richards equation was developed for this kind of flow and it is a pressure and saturation based formation. The pressure mentioned in this

situation includes the so called capillary pressure, which is brought by the surface tension caused by the interaction of the soil and the fluid phases. The fluid saturation has strong influence on the capillary pressure.

The Richards equation can be expressed by (Richards, 1931)

$$\frac{\partial\theta}{\partial t} = \frac{\partial}{\partial x}[K(\theta)\frac{\partial\psi}{\partial x}] + \frac{\partial}{\partial y}[K(\theta)\frac{\partial\psi}{\partial y}] + \frac{\partial}{\partial z}[K(\theta)(\frac{\partial\psi}{\partial z} + 1)] \tag{5.10}$$

where $\theta[-]$ is the volumetric water content (moisture content), $t[T]$ is time, x, y, and $z[L]$ are the spatial coordinates, $K[LT^{-1}]$ is the hydraulic conductivity, and $\psi[L]$ is the pressure head. There's no closed-form analytical solution to this non-linear partial differential equation.

5.2.2 Effect of saturation

The volumetric water content $\theta[-]$ is defined as

$$\theta = \frac{V_w}{V_T} \tag{5.11}$$

where $V_T[L^3]$ is the total volume and $V_T = V_s + V_v = V_s + V_w + V_a$, $V_s[L^3]$ is the volume of solid phase, $V_v[L^3]$ is the volume of void or pore space, $V_w[L^3]$ is the volume of water, and $V_a[L^3]$ is the volume of air.

The water saturation $S[-]$ is

$$S = \frac{V_w}{V_v} \tag{5.12}$$

And porosity $n[-]$ is

$$n = \frac{V_v}{V_T} \tag{5.13}$$

Thus the relationship between the volumetric water content and the water saturation is

$$\theta = nS \tag{5.14}$$

The effective water saturation $S_e[-]$ is defined as

$$S_e = \frac{\theta - \theta_r}{n - \theta_r} \tag{5.15}$$

where $\theta_r[-]$ is residual water content, defined as the water content for which the gradient $d\theta/dh$ is zero.

The hydraulic conductivity K in the unsaturated porous medium is modified from that in Darcy's equation (see section 2.1, equation 2.3)

$$K = kk_r \frac{\rho g}{\mu} \tag{5.16}$$

where $k_r[-]$ is called relative hydraulic conductivity, which depends on the fluid phase saturation, $k[L^2]$ is intrinsic permeability, $\rho[ML^{-3}]$ is density of water, $g[LT^{-2}]$ is gravitational acceleration, and $\mu[MT^{-1}L^{-1}]$ is the dynamic viscosity of water.

The relative hydraulic conductivity can be empirically described by several formulae, of which the van Genuchten model (van Genuchten, 1980) is popularly adopted. It is formulated as

$$k_r = {S_e}^{1/2}[1 - (1 - {S_e}^{1/m})^m]^2 \tag{5.17}$$

where $m[-]$ is an empirical parameter depends on soil type.

5.2.3 Effect of capillary pressure

The relationship between the hydraulic head h and the pressure head ψ is

$$h = \psi + z \tag{5.18}$$

where $z[L]$ is elevation head. The pressure head ψ is to represent the internal energy of a fluid due to the pressure exerted on its container. It is formulated as

$$\psi = \frac{P}{\rho g} \tag{5.19}$$

where P $[ML^{-1}T^{-2}]$ is pressure. In the unsaturated zone exist two phases of fluid, air and water. If one of the two phases (typically the air) is assumed to have a constant

pressure, then P is given by the capillary pressure $p_c[ML^{-1}T^{-2}]$ that

$$p_c = -P \tag{5.20}$$

As mentioned, capillary pressure is strongly affected by fluid saturation. Many researches were carried out and the relationship between these two items was mathematically described. Here the van Genuchten model (van Genuchten, 1980) is adopted and the capillary pressure is formulated as

$$p_c = \frac{\rho g}{\alpha}({S_e}^{-1/m} - 1)^{1/r} \tag{5.21}$$

where $\alpha[M^{-1}LT^2]$ and $r[-]$ are empirical parameters and

$$m = 1 - \frac{1}{r} \tag{5.22}$$

5.2.4 Richards flow in 1D porous medium

A soil column infiltration experiment (Warrick et al., 1971) is numerically simulated with 1D Richards flow in unsaturated porous medium. The height of the soil column is $2m$. Constant pressure are maintained on the top and bottom of the column with the value $0Pa$ and $-21500Pa$, respectively. The whole domain has uniform initial pressure of $-21500Pa$ and saturation of 0.455. According to equation (5.21) and equation (5.17), the capillary pressure and relative permeability are functions of the effective saturation and the relationships of these parameters are plotted in Fig. 5.5.

The whole domain is considered as a homogeneous porous medium. Material properties of the soil column infiltration model are shown in Tab. 5.3.

The simulation results of pressure and saturation distribution along the column at various time steps are shown in Fig. 5.6 and Fig. 5.7.

The volumetric flux is determined by Darcy's law. For the solute transport, particles are injected to the top of the soil column as a slug input. Particles take use of the velocity field obtained by Richards and Darcy equations. Relative parameters are listed in Tab. 5.4. The breakthrough curve of solute concentration (represented by particle number) at the depth

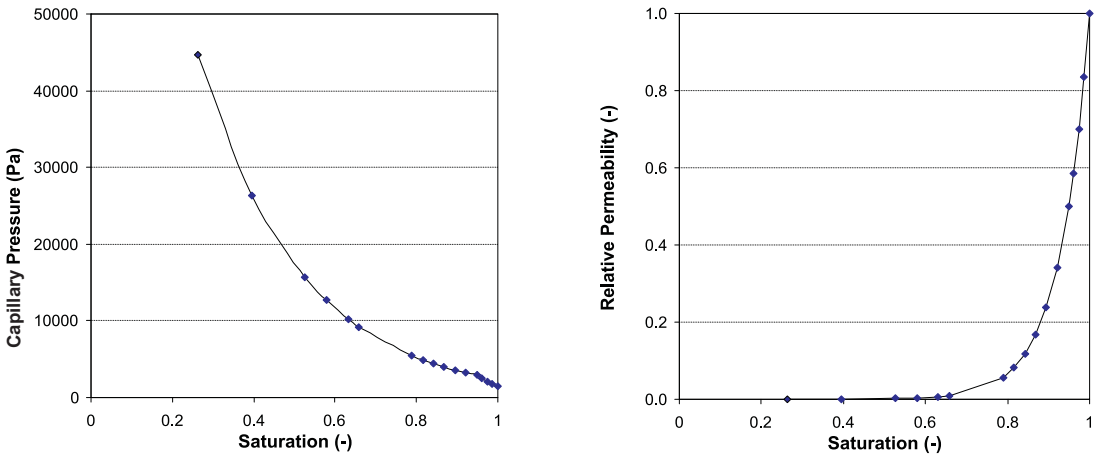

Figure 5.5: Distribution of capillary pressure (l) and relative permeability(r) relative to saturation

Table 5.3: Material properties for the infiltration model

Symbol	Parameter	Value	Unit
P_t	Pressure (top)	0	Pa
P_b	Pressure (bottom)	-21500	Pa
L	Column height	2	m
k	Intrinsic permeability	4.46×10^{-13}	m^2
n	Porosity	0.38	–
p_c	Capillary pressure	Curve in Fig. 5.5(l)	Pa
k_{rel}	Relative permeability	Curve in Fig. 5.5(r)	-

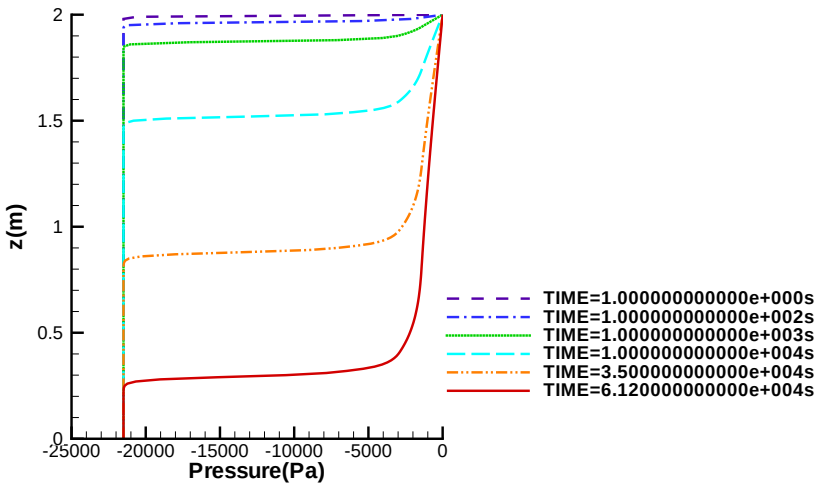

Figure 5.6: Pressure distribution along the soil column at different time steps

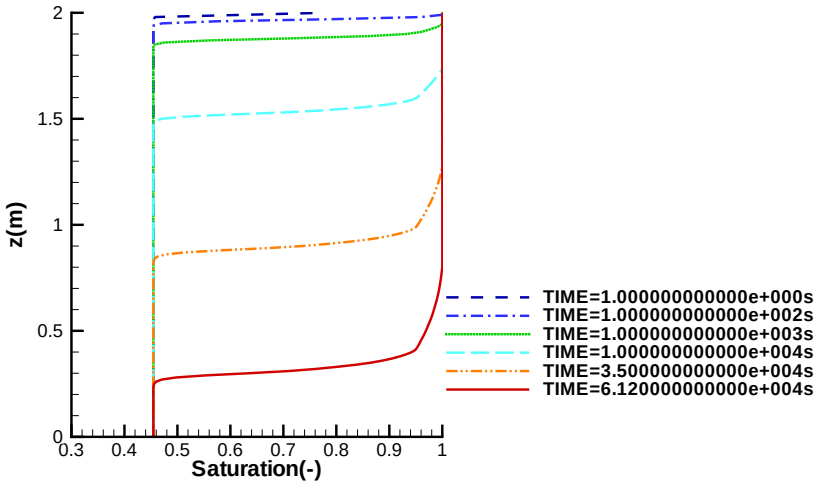

Figure 5.7: Saturation distribution along the soil column at different time steps

of $1.5m$ from the top of the column ($z = 0.5m$) is shown in Fig. 5.8.

Table 5.4: Model properties for particles in the soil column

Symbol	Parameter	Value	Unit
α_L	Longitudinal dispersivity	2.7×10^{-4}	m
D_d	Diffusion coefficient	1.16×10^{-7}	m^2s^{-1}

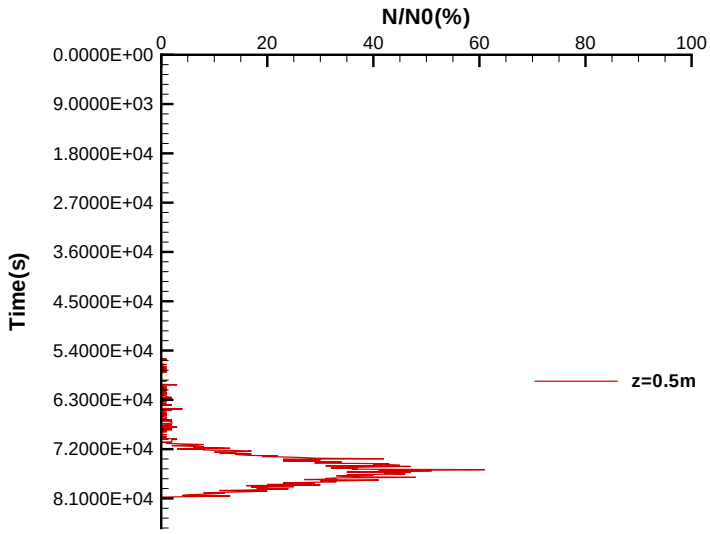

Figure 5.8: Breakthrough curve at $z = 0.5m$

It takes $7.57 \times 10^4 s(21h)$ for the particles to reach the observation point. While the pressure and saturation's penetration to the identical point takes about $6.12 \times 10^4 s(17h)$. This retardation phenomenon was observed in the experiment as well, that the solute was not detected in the advancing wetting front but lagged behind.

Chapter 6

Model applications

6.1 Pore scale modeling

Simulation of fluid flow in porous media can be implemented in macroscale, for example, the utilization of Darcy's law in groundwater flow simulation, or Forchheimer flow with higher velocity, and Richard flow in unsaturated zone. It can also be described in relatively smaller scale, for instance, pore scale. Macroscale simulations take use of macroscopic properties in the continuum scale - porosity, water content, hydraulic conductivity, specific storage, and so on. Pore scale simulations, on the other hand, focus on the investigation of microscopic properties, like permeability, capillary pressure. Numerical simulation of microscale flow in pore space helps to quantify and visualize the development of pore scale fluid preferential flow paths through the porous medium. The proposed RWPT method takes use of the velocity field obtained from the pore scale flow simulation to advect the particles in the pore space.

6.1.1 Navier-Stokes equations

In the simulation of water movement in the connected pore spaces of the porous medium, incompressible Navier-Stokes equations are popularly adopted. The Navier-Stokes equations are physical equations derived from the theory of hydrodynamics in microscale and used to describe the flow of Newtonian fluids of nearly constant density. Assuming that

all the stresses in the flow field are carried out by the porous medium and the water's density and viscosity are constant, the simplified form of the incompressible Navier-Stokes equation can be expressed by (Bear, 1988; Whitaker, 1966)

$$\rho\left(\frac{\partial \mathbf{v}}{\partial t} + \mathbf{v}\cdot\nabla\mathbf{v}\right) = -\nabla P + \mu\nabla^2\mathbf{v} + \mathbf{f} \tag{6.1}$$

where $\rho[ML^{-3}]$ is density of water, $\mathbf{v}[LT^{-1}]$ is velocity, $t[T]$ is time, $P[ML^{-1}T^{-2}]$ is pressure, $\mu[MT^{-1}L^{-1}]$ is the dynamic viscosity of water, $\mathbf{f}[ML^{-2}T^{-2}]$ represents body forces, and ∇^2 is vector Laplacian.

And to complete the system, an additional continuity equation derived from the law of mass conservation can be written as

$$\nabla\cdot\mathbf{v} = 0 \tag{6.2}$$

The Navier Stokes equations are nonlinear partial differential equations and are difficult to solve directly. Several approaches are developed to get the solution to these equations. In the open source CFD toolbox OpenFOAM, the SIMPLE (Semi-Implicit Method for Pressure-Linked Equations) algorithm is implemented and allows to couple the Navier Stokes equations with an iterative procedure.

6.1.2 Pore space computational mesh generation

To establish a numerical model, not only a detailed understanding of the flow behavior in the pore space is needed, an accurate and realistic characterization of the structure of the pore space is significant as well. In this work, the pore space computational mesh is generated by the utilization of CGAL and settleDyn.

The Computational Geometry Algorithms Library (CGAL, `http://www.cgal.org`) offers data structures and algorithms for the computational mesh generation. "The goal of the CGAL Open Source Project is to provide easy access to efficient and reliable geometric algorithms in the form of a C++ library."(The CGAL Project, 2012) The support library offers geometric object generators and spatial sorting functions, as well as a matrix search framework and a solver for linear and quadratic programs. CGAL generates meshes that

discretize 3D domains.

Settle dynamics (settleDyn for short, `http://naumov.de/settleDyn/`) is a sedimentation process simulator. It is capable of generating loose sand-like structures from given particle forms and statistical distributions.

To generate a mesh, first a polyhedral domain (Fig. 6.1a) is prepared, and a tetrahedral mesh of the domain is generated with CGAL. For the grains that inside of the domain, a 3D image (Fig. 6.1b) is used, which is very flexible, can be obtained from micro-CT scans or generated manually. The structure of the grains, or the pore space, is generated with settleDyn. Grains are represented by polyhedrons.

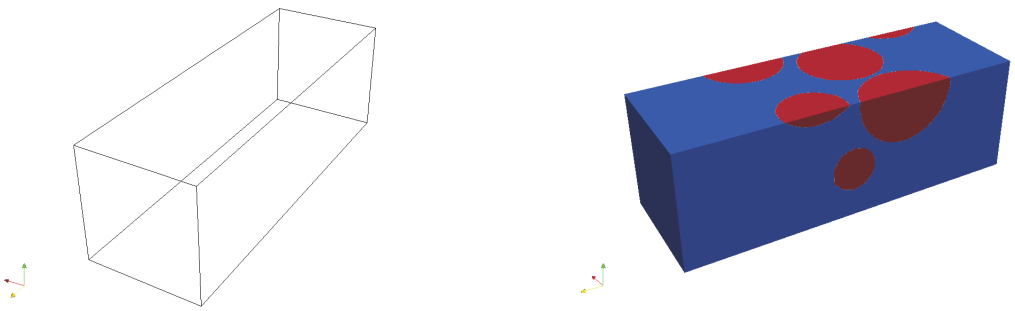

(a) Domain outline (b) Grain image

Figure 6.1: CGAL mesh generation

Secondly, use the grain mesh to refine the domain mesh with CGAL's mesh refining algorithm. Using the Delaunay triangulation, with sub domain labels, the labeled tetrahedral mesh with embedded grains (Fig. 6.2) is generated.

6.1.3 Particle tracking in pore scale model

This section describes a joint work with Dmitri Naumov (Naumov, 2013). An artificial pore scale model is established for the simulation of potential flow and particle tracking in the pore space. The pore scale model is based on a realistic description of the pore space and a detailed analysis of displacement mechanisms to predict pore scale fluid flow properties.

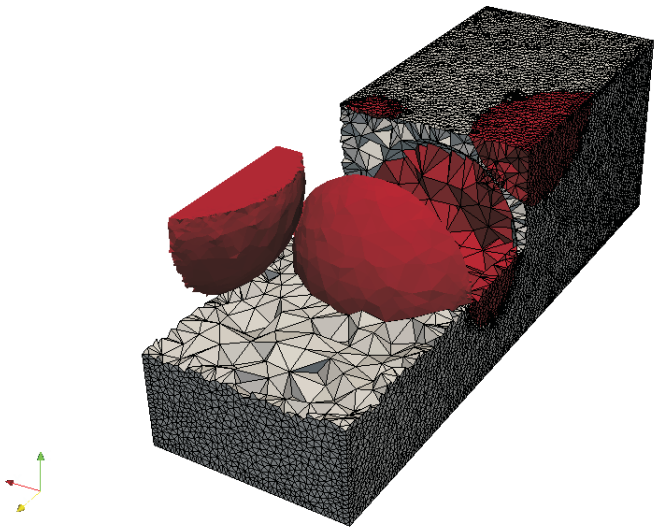

Figure 6.2: Mesh with embedded grains

The calculation domain is a rectangular parallelepiped with several grains inside (see Fig. 6.2). The grains' sizes are not uniform and grains are randomly distributed among the domain. The pore space is discretized with tetrahedral elements and the inside spaces of the grains are discretized as well.

The flow field is simplified to potential flow which results from Darcy's law and is commonly used in large scale problems when the groundwater flow equation is simplified to Laplace's equation. On the inlet and outlet boundary, Dirichlet boundary conditions are adopted that constant hydraulic heads are set on both front and back surfaces. Other surfaces are set to be no-flow boundaries that fluid cannot pass the boundary and adjacent flow lines are parallel to the boundary surface. The pore space is treated as a medium which is set to be homogeneous and isotropic. Fig. 6.3 shows the hydraulic head isosurfaces of the calculation domain.

In the potential flow, the hydraulic head gradient has a direction that is always perpendicular to the equipotential lines. As this is an isotropic medium, the direction of fluid

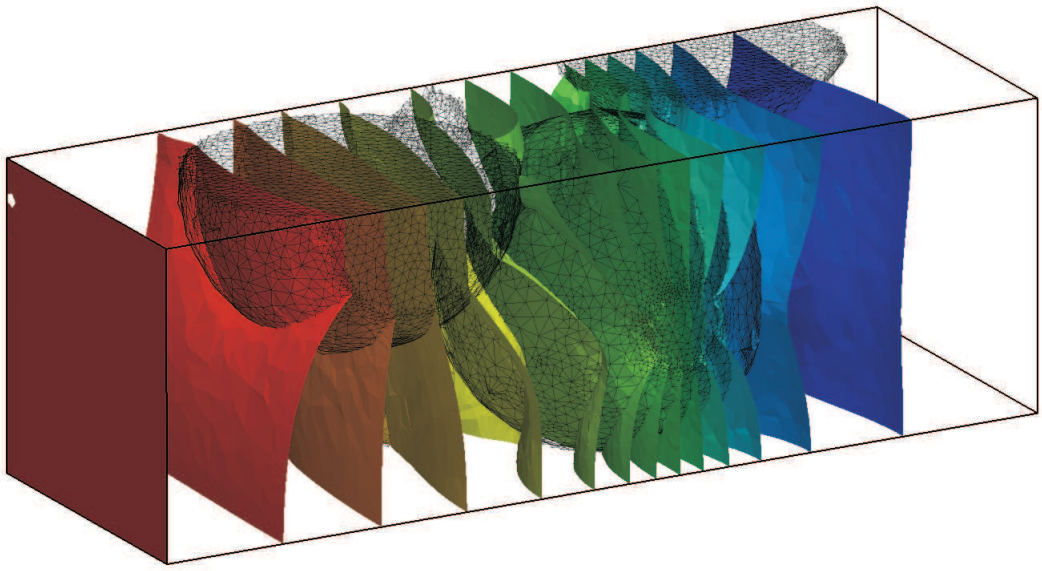

Figure 6.3: Hydraulic head isosurfaces in domain with grains - potential flow

flow is parallel to the hydraulic head gradient, i.e., flow lines will cross the hydraulic head isosurfaces at right angles.

Particles are released to the domain from an area close to the inlet boundary for a constant time. Fig. 6.3 shows the simulation results of particles' distribution over time.

The particles are carried along by the fluid and move in the pore space. The "random walk" property allows the particles to digress from the flow line to some extent. Some of the particles enter the dead end of the pore space where the velocity is extremely low. Some hit to the surface of the grains and get captured because the velocity there is close to zero. The simulation results show the advantage of the proposed RWPT method that it is capable to describe the detailed flow properties.

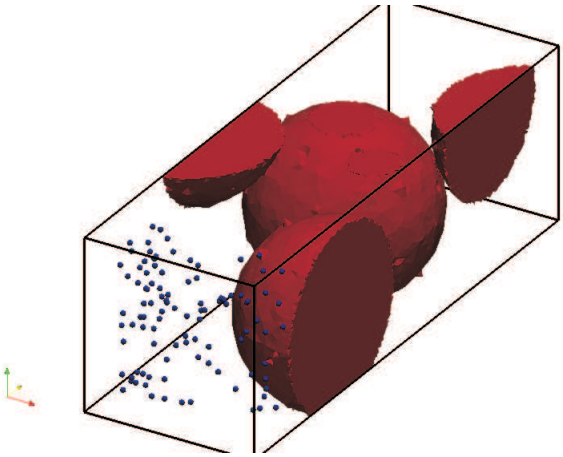

(a) 0

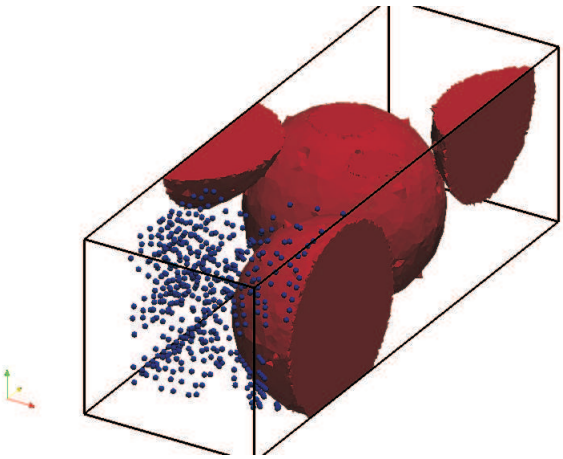

(b) 50

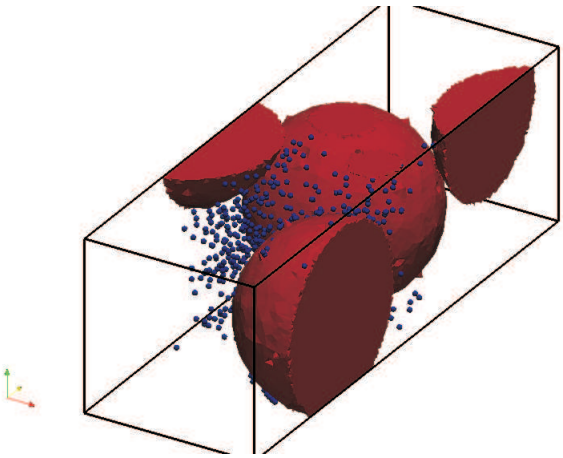

(c) 100

Figure 6.4: Particle clouds in domain with embedded grains

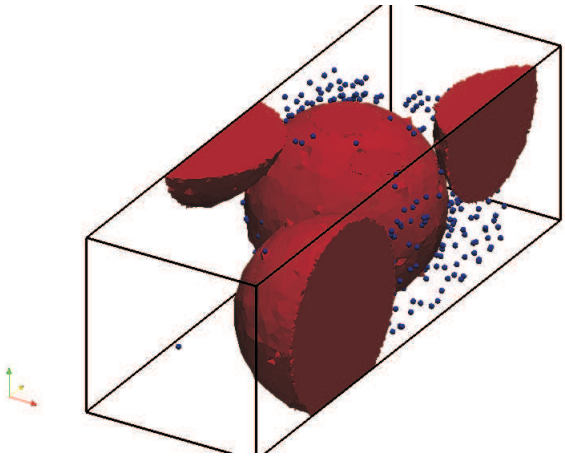

(d) 150

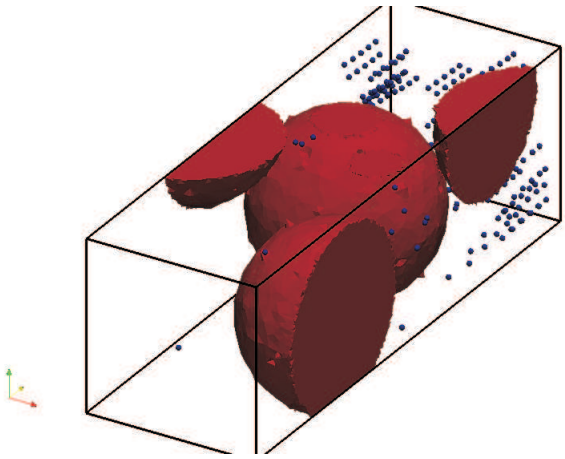

(e) 200

Figure 6.3: Continued: Particle clouds in domain with embedded grains

6.2 Nankou site of Beijing Plain

One of the most important applications of the random walk particle tracking method is to model solute transport in aquifers and find the bulk-averaged characteristics like the contaminant plume. In this section a two dimensional groundwater flow and solute transport model is established based on a cite study and estimated with heterogeneous material properties.

The study site is located in Nankou area which is on the northwest edge of the Beijing Plain in China (Fig. 6.4). Due to the large urbanization since 1990s, population and constructions in this area grow rapidly, which brings in an increment of the water consumption and consequent contamination. The main water supply in this area is from the exploitation of groundwater; meanwhile, the annual precipitation in recent years is relatively small comparing to the historical records, thus leading to a drawdown of the groundwater table. A heavily contaminated patch with high concentration nitrate was found in the north part of the study site which is the upstream of groundwater flow. For the purpose of contamination remediation and water resources management, the study site was established and observation data have been recorded and analyzed.

In the PhD thesis of Sun (Sun, 2011), a transient groundwater flow model was established to simulate the local hydrogeological system, using the software of OpenGeoSys (OGS). The geology of the study area is complex and the identification of parameters is essential to the accuracy of the model. The parameter calibration was carried out with software PEST which makes use of the nonlinear least-squares inverse method and can be integrated with other groundwater modeling simulators. The well-calibrated model successfully generated results of transient groundwater system under pumping stress and drought conditions (Sun et al., 2011).

In the north part of the study site, high concentration of nitrate was detected in the groundwater from an observation well. A groundwater quality monitoring network was established to measure nitrate concentration in other observation wells in the study site. Figure 6.5 shows the nitrate concentration distribution in this area in Feb. 2010. A fertilizer factory was found to be the pollution source since it was producing ammonia and releasing waste water with ammonium to the nearby river for nearly two decades. In Sun's thesis,

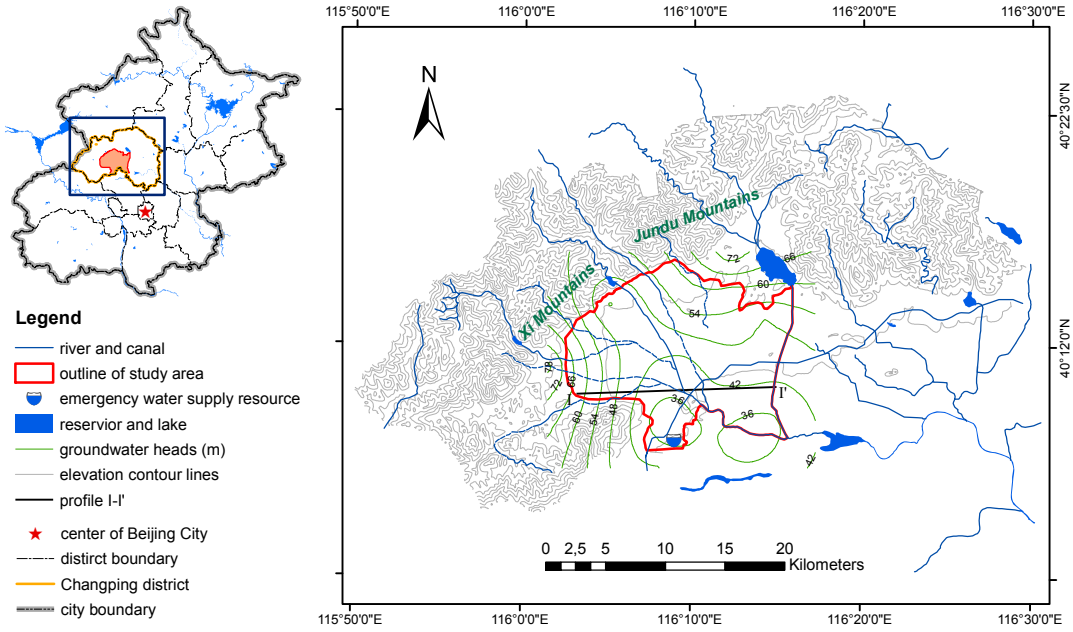

Figure 6.4: Location of the Nankou study site (Sun, 2011)

a contaminant transport model was established in a redefined domain that is close to the observation well with high concentration (Fig. 6.6). It is a 2D heterogeneous model and the hydraulic conductivity properties are generated with GSTAT based on the data obtained from pumping test results.

In this work, a RWPT model is established for the purpose of testifying the capability of particle tracking method working in real world applications by comparing the simulation result with the FEM method.

Figure 6.7 shows the result of FEM simulation of nitrate concentration distribution after 30 years and Figure 6.8 is the result from RWPT method. It is a primary result because only the fertilizer factory is considered as pollution source.

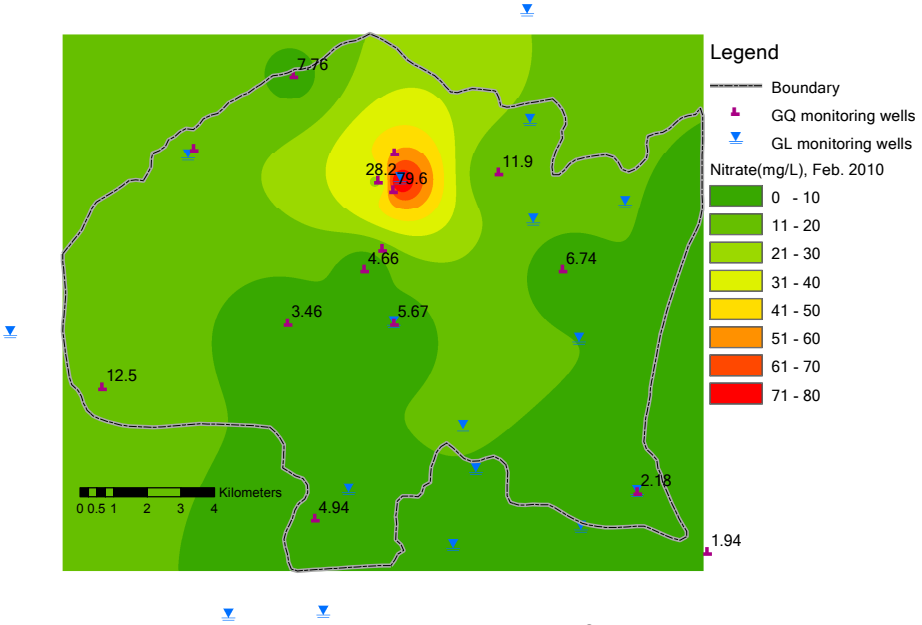

Figure 6.5: Nitrate concentration distribution of Nankou study site (Sun, 2011)

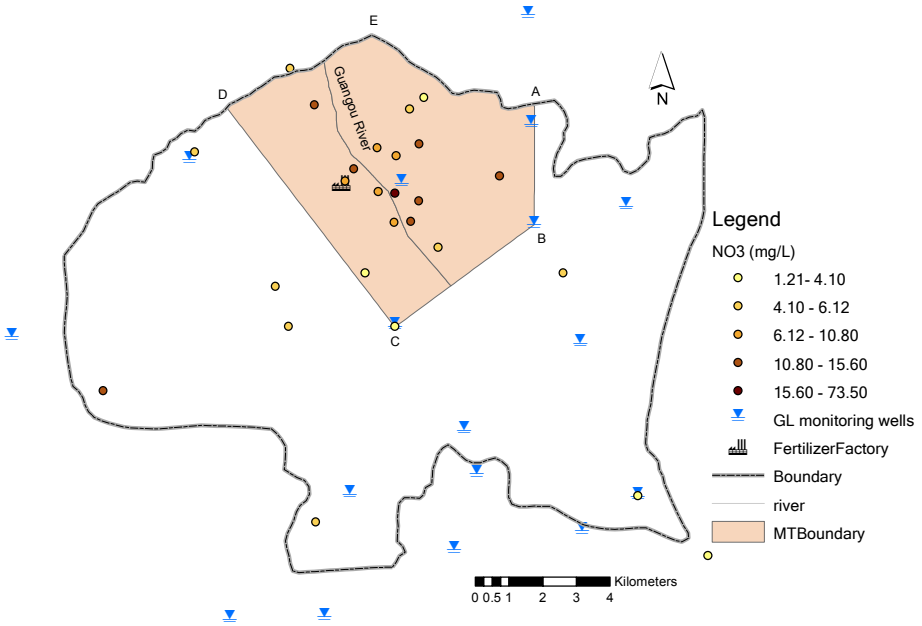

Figure 6.6: Calculation domain for contaminant transport model (Sun, 2011)

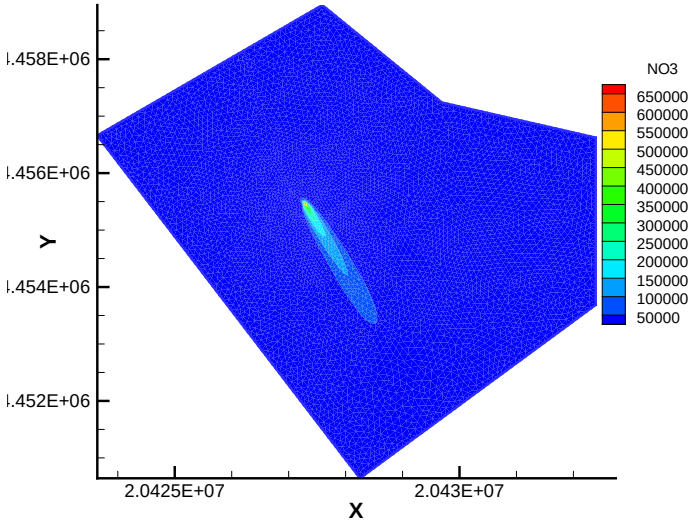

Figure 6.7: FEM simulation of nitrate concentration distribution

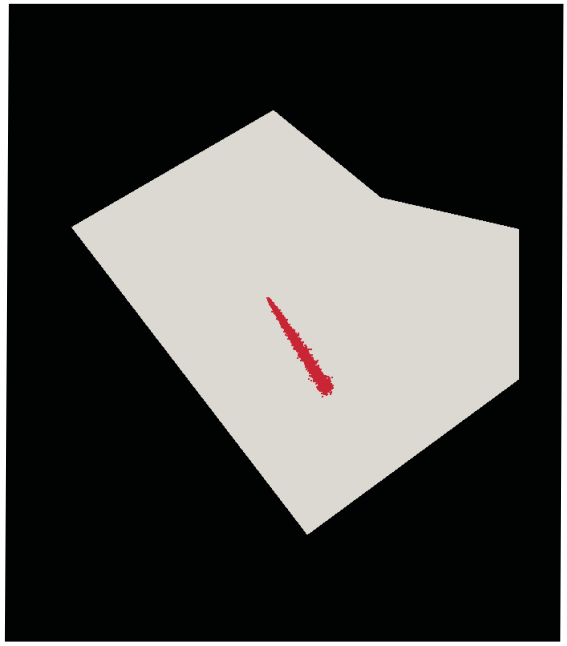

Figure 6.8: Particle tracking of nitrate concentration distribution

Chapter 7

Summary and outlook

Random walk particle tracking (RWPT) method provides a computationally effective way to characterize solute transport process in porous media. In this work, an object-oriented scientific software platform OpenGeoSys (OGS) was adopted for the simulation and visualization of the complex behavior of particles. Finite element method was used for the calculation of the velocity field which is necessary for the determination of the displacement of the particles through space.

The RWPT method has been used in the simulation of the hydraulic process, diffusion and dispersion as it is proved to be well suited for such studies. In this work, efforts were taken to search for the solution to simulate the retardation and decay processes in order to investigate the effects that appear in the contaminant plume evolution. Expressions for the effective coefficients governing the solute transport are derived for retardation model, based on a two-rate sorption-desorption approach.

The RWPT model was verified by several benchmarks of solute transport with Darcy flow in one-, two-, and three-dimensional homogeneous and heterogeneous porous media to analysis the accuracy of the method with comparison to the analytical solutions. The RWPT model produced the results in good agreement with the analytical solutions. Forchheimer flow and Richards flow were adopted for the particle tracking as well. Two applications were described which shows the capability of the method to work in real-world.

The advantage of this method is mainly reflected in its capability of more detailed description for flow and transport processes comparing to the traditional finite element

method. The limitation that it is computational expensive can be overcome by parallel computing. The applications of this method to various aspects are to be expected.

Appendix A

Publications list

Journal publications and conference proceedings

1. **Y. Y. Sun**, C. H. Park, W. Wang, and O. Kolditz. Simulation of solute transport in 3D porous media using random walk particle tracking method. In proceedings of the II International Conference on Particle-based Methods - Fundamentals and Applications (PARTICLES 2011), Barcelona, Spain, 26-28 October, 2011. CIMNE, Barcelona, ISBN: 978-84-89925-67-0, pages 627-638.

2. O. Kolditz, S. Bauer, L. Bilke, N. Boettcher, J. O. Delfs, T. Fischer, U. J. Goerke, T. Kalbacher, G. Kosakowski, C. I. McDermott, C. H. Park, F. Radu, K. Rink, H. Shao, H. B. Shao, F. Sun, **Y. Y. Sun**, A. K. Singh, J. Taron, M. Walther, W. Wang, N. Watanabe, Y. Wu, M. Xie, W. Xu, and B. Zehner. OpenGeoSys: an open-source initiative for numerical simulation of thermo-hydro-mechanical/chemical (THM/C) processes in porous media. *Environmental Earth Sciences*, 67(2): 589-599. 2012.

Book chapters

1. S. Bauer, C. Beyer, C. I. McDermott, G. Kosakowski, S. Krug, C. H. Park, G. Pichot, H. B. Shao, **Y. Y. Sun**, J. Taron. Mass transport. In O. Kolditz, U. J. Goerke, H. Shao, and W. Wang, editors, *Thermo-Hydro-Mechanical-Chemical Processes in Porous Media*. Springer, Berlin, 2012. ISBN: 978-3-642-27176-2.

REFERENCES

S.W. Ahlstrom and H.P. Foote. Multi-component mass transport model: theory and numerical implementation (discrete parcel random walk version). Technical report, Battelle Pacific Northwest Lab., Richland, Washington, 1977.

G.M. Amdahl. Validity of the single processor approach to achieving large scale computing capabilities. *AFIPS conference proceedings*, 30:483–485, 1967.

M. Balhoff, A. Mikelic, and M. Wheeler. Polynomial filtration laws for low reynolds number flows through porous media. *Transport in Porous Media*, 81:35–60, 2010.

C. Barber, C.J. Otto, L.E. Bates, and K.J. Taylor. Evaluation of the relationship between land-use changes and groundwater quality in a water-supply catchment, using gis technology: the gwelup wellfield, western australia. *Hydorgeol. Jour.*, 4(1):6–19, 1996.

J. Bear. *Hydraulics of groundwater*. McGraw-Hill, New York, 1979.

J. Bear. *Dynamics of fluids in porous media*. Dover, New York, 1988.

J. Bensabat, Q.L. Zhou, and J. Bear. An adaptive pathline-based particle tracking algorithm for the eulerian-lagrangian method. *Advances in Water Resour.*, 23(4):383–397, 2000.

D.A. Benson and M.M. Meerschaert. A simple and efficient random walk solution of multi-rate mobile/immobile mass transport equations. *Advances in Water Resour.*, 32:532–539, 2009.

B. Berkowitz, G. Kosakowski, G. Margolin, and H. Scher. Application of continuous time random walk theory to tracer test measurements in fractured and heterogeneous porous media. *Ground Water*, 39(4):593–604, 2001.

T.H. Chilton and A.P. Colburn. Pressure drop in packed tubes. *Ind. & Engng. Chem.*, 23 (8):913–919, 1931.

A. Cortis, T. Harter, L. Hou, and E.R. Atwill. Transport of *Cryptosporidium* in porous media: Long-term elution experiments and continuous time random walk filtration modeling. *Water Resour. Res.*, 42(W12S13):12pp, 2006.

G. De Josselin de Jong. Longitudinal and transverse diffusion in granular deposits. *Trans. Am. Geophys. Union*, 39(1):67–74, 1958.

F.A.L. Dullien and M.I.S. Azzam. Flow rate - pressure gradient measurements in periodically nonuniform capillary tubes. *A. I. Ch. E. J.*, 19:222–229, 1973.

S. Ergun. Fluid flow through packed columns. *Chem. Engng. Prog.*, 48(2):8994, 1952.

S. Ergun and A. A. Orning. Fluid flow through randomly packed columns and fluidized beds. *Ind. & Engng. Chem.*, 41(6):11791184, 1949.

G.H. Fancher and J.A. Lewis. Flow of simple fluids through porous materials. *Ind. & Engng. Chem.*, 25(10):1139–1147, 1933.

D. Fernandez-Garcia and X. Sanchez-Vila. Optimal reconstruction of concentrations, gradients and reaction rates from particle distributions. *Jour. of Contamin. Hydrol.*, 120-121: 99–114, 2011.

P. Forchheimer. *Wasserbewegung durch Boden*. Zeitschrift des Vereines Deutscher Ingenieur, 1901.

L. Jr. Green and P. Duwez. Fluid flow through porous metals. *J. Appl. Mech.*, page 3945, 1951.

T. Harter and S. Wagner. Colloid transport and filtration of *Cryptosporidium parvum* in sandy soils and aquifer sediments. *Environ. Sci. Technol.*, 34:62–70, 2000.

A.E. Hassan and M.M. Mohamed. On using particle tracking methods to simulate transport in single-continuum and dual continua porous media. *Jour. of Hydrol.*, 275:242–260, 2003.

S.M. Hassanizadeh and W.G. Gray. High velocity flow in porous media. *Transport Porous Media*, 2:521531, 1987.

H. Hoteit, R. Mose, A. Younes, F. Lehmann, and Ph. Ackerer. Three-dimensional modeling of mass transfer in porous media using the mixed hybrid finite elements and the random-walk methods. *Mathe. Geology*, 34(4):435–456, 2002.

P.S. Huyakorn and G.F. Pinder. *Computational methods in subsurface flow*. Academic, San Diego, Calif, 1983.

P.H. Israelsson, Y.D. Kim, and E.E. Adams. A comparison of three lagrangian approaches for extending near field mixing calculations. *Environ. Model. & Soft.*, 21:1631–1649, 2005.

K. Ito. On stochastical differential equations. *American Mathematical Society*, 4:289–302, 1951.

J.A. Izbicki, C.L. Stamos, T. Nishikawa, and P. Marti. Comparison of ground-water flow model particle-tracking results and isotopic data in the mojave river ground-water basin, southern california, usa. *Jour. of Hydrol.*, 292:30–47, 2004.

W.P. Johnson, K.A. Blue, and B.E. Logan. Modeling bacterial detachment during transport through porous media as a residence-time-dependent process. *Water Resour. Res.*, 31: 2649–2658, 1995.

G. Karypis and V. Kumar. A parallel algorithm for multi-level graph partitioning and sparse matrix ordering. *Journal of Parallel and Distributed Computing*, 48(1):71–95, 1998.

W. Kinzelbach. *Groundwater Modelling*. Elsevier, Amsterdam, 1986.

W. Kinzelbach. The random-walk method in pollutant transport simulation. *NATO ASI Ser*, Ser.(C224):227–246, 1988.

P.K. Kitanidis. Particle-tracking equations for the solution of the advection-dispersion equation with variable coefficients. *Water Resour. Res.*, 30(11):3225–3227, 1994.

O. Kolditz. *Computational Methods in Environmental Fluid Mechanics*. Springer, Berlin, 2002.

O. Kolditz and S. Bauer. A process-oriented approach to computing multi-field problems in porous media. *Jour. of Hydroinfor.*, 6:225–244, 2004.

O. Kolditz, S. Bauer, L. Bilke, and N. Boettcher. Opengeosys: an open-source initiative for numerical simulation of thermo-hydro-mechanical/chemical (thm/c) processes in porous media. *Environ. Earth Sci.*, 67(2):589–599, 2012a.

O. Kolditz, U. Goerke, H. Shao, and W. Wang. *Benchmarks and examples for Thermo-Hydro-Mechanical-Chemical processes in porous media*. Springer, Berlin, 2012b.

L.F. Konikow and J.D. Bredehoeft. *Computer model of two-dimensional solute transport and dispersion in ground water*. U.S. Geological Survey, Techniques of Water-Resources Investigations, Book 7, Chapter C2, 90p, 1978.

E.M. LaBolle, G.E. Fogg, and A.F.B. Tompson. Random-walk simulation of transport in heterogeneous porous media: Local mass-conservation problem and implementation methods. *Water Resour. Res.*, 32(3):583–593, 1996.

E.M. LaBolle, J. Quastel, G.E. Fogg, and J. Gravner. Diffusion processes in composite porous media and their numerical integration by random walks: generalized stochastic differential equations with discontinuous coefficients. *Water Resour. Res.*, 36(3):651–662, 2000.

G. Liu, C. Zheng, and S.M. Gorelick. Limits of applicability of the advection-dispersion model in aquifers containing connected high-conductivity channels. *Water Resour. Res.*, 40(W08308):doi:10.1029/2003WR002735, 2004.

R. Mettier, G. Kosakowski, and O. Kolditz. Influence of small-scale heterogeneities on contaminant transport in fractured crystalline rock. *Ground Water*, 44(5):687–696, 2006.

D. Naumov. *Flow in Porous Media: Numerical Porescale Modelling and Visualization*. PhD thesis, TU Dresden, 2013.

E.W. North, Z. Schlag, R.R. Hood, and L. Zhong. Vertical swimming behavior influences the dispersal of simulated oyster larvae in a coupled particle-tracking and hydrodynamic model of chesapeake bay. *Mar. Ecol. Prog. Ser.*, 359:99–115, 2008.

A. Ogata and R.B. Banks. A solution of the differential equation of longitudinal dispersion in porous media. Technical report, USGS, Washington, D.C., 1961.

C.-H. Park and M.M. Aral. Sensitivity of the solution of the elder problem to density, velocity and numerical perturbations. *Jour. of Contamin. Hydrol.*, 92:33–49, 2007.

C.-H. Park and P.M. Huck. A conceptual model for *Cryptosporidium* transport in watersheds. *Water Qual. Res. J. Can.*, 38(1):77–113, 2003.

C.-H. Park, C. Beyer, S. Bauer, and O. Kolditz. Using global node-based velocity in random walk particle tracking in variably saturated porous media: application to contaminant leaching from road constructions. *Environ. Geol.*, 55:1755–1766, 2008a.

C.H. Park, C. Beyer, S. Bauer, and O. Kolditz. A study of preferential flow in heterogeneous media using random walk particle tracking. *Geosci. Jour.*, 12(3):285–297, 2008b.

A.R. Piggott and D. Elsworth. Laboratory assessment of the equivalent apertures of a rock fracture. *Geophysical Research Letters*, 20(13):1387–1390, 1993.

C.D. Pint, R.J. Hunt, and M.P. Anderson. Flowpath delineation and ground water age, allequash basin, wisconsin. *Ground Water*, 41(7):895–902, 2003.

T.A. Prickett, T.G. Naymik, and C.G. Lonnquist. *A "Random-Walk" Solute Transport Model for Selected Groundwater Quality Evaluations*, volume Bulletin 65. Illinois State Water Survey, Champaign, 1981.

F.A. Radu, N. Suciu, J. Hoffmann, A. Vogel, O. Kolditz, C.-H. Park, and S. Attinger. Accuracy of numerical simulations of contaminant transport in heterogeneous aquifers: A comparative study. *Advances in Water Resour.*, 34:47–61, 2011.

L.A. Richards. Capillary conduction of liquids through porous mediums. *Physics*, 1(5): 318–333, 1931.

B.A. Robinson, Z.V. Dash, and G. Srinivasan. A particle tracking transport method for the simulation of resident and flux-averaged concentration of solute plumes in groundwater models. *Comput. Geosci.*, 14(4):779–792, 2010.

M.A. Robinson and W.G. Reay. Ground water flow analysis of a mid-atlantic outer coastal plain watershed, virginia, u.s.a. *Ground Water*, 40(2):123–131, 2002.

D.W. Ruth and H. Ma. On the derivation of the forchheimer equation by means of the averaging theorem. *Transport in Porous Media*, 7:255–264, 1992.

P. Salamon, D. Fernandez-Garcia, and J.J. Gomez-Hernandez. A review and numerical assessment of the random walk particle tracking method. *Jour. of Contamin. Hydrol.*, 87:277–305, 2006.

A.E. Scheidegger. Statistical hydrodynamics in porous media. *Jour. of Appl. Physics*, 25 (8):994–1001, 1954.

H. Shao. *Modelling reactive transport processes in porous media*. PhD thesis, TU Dresden, 2010.

W.T. Sloan and J. Ewen. Modelling long-term contaminant migration in a catchment at fine spatial and temporal scales using the up system. *Hydrol. Process.*, 13:823–846, 1999.

G. Srinivasan, D.M. Tartakovsky, M. Dentz, H. Viswanathan, B. Berkowitz, and B.A. Robinson. Random walk particle tracking simulations of non-fickian transport in heterogeneous media. *Jour. of Comput. Physics*, 229(11):4304–4314, 2010.

S.-W. Suh. A hybrid approach to particle tracking and eulerian-lagrangian models in the simulation of coastal dispersion. *Environ. Model. & Soft.*, 21:234–242, 2004.

H. Suk and G.-T. Yeh. Development of particle tracking algorithms for various types of finite elements in multi-dimensions. *Comput. & Geosci.*, 36:564–568, 2010.

F. Sun. *Computational hydrosystem analysis: applications to the Meijiang and Nankou catchments in China*. PhD thesis, TU Dresden, 2011.

F. Sun, H. Shao, T. Kalbacher, and W. Wang. Groundwater drawdown at nankou site of beijing plain: model development and calibration. *Environ. Earth Sci.*, 64(5):1323–1333, 2011.

The CGAL Project. {*CGAL*} *User and Reference Manual*. CGAL Editorial Board, 4.1 edition, 2012.

A.F.B. Tompson and L.W. Gelhar. Numerical simulation of solute transport in three-dimensional, randomly heterogeneous porous media. *Water Resour. Res.*, 26(10):2541–2562, 1990.

A.F.B. Tompson, R.D. Falgout, S.G. Smith, W.J. Bosl, and S.F. Ashby. Analysis of subsurface contaminant migration and remediation using high performance computing. *Advances in Water Resour.*, 22(3):203–221, 1998.

G. Uffink. *Modeling of solute transport with the random walk method. In: Custodio, E., Gurgui, A., Lobo Ferreira, J.P.(Eds.), Groundwater flow and quality modeling*. Reidel, Norwell, Mass, 1987.

M. van Genuchten. A closed-form equation for producing the hydraulic conductivity of unsaturated soils. *Soil Sci. Am. J.*, 44:892–898, 1980.

M. van Genuchten. Analytical solutions for chemical transport with simultaneous adsorption, zero-order production and first order decay. *Jour. of Hydrol.*, 49:213–233, 1981.

W. Wang, G. Kosakowski, and O. Kolditz. A parallel finite element scheme for thermo-hydro-mechanical (thm) coupled problems in porous media. *Comput. Geosci.*, 35:1631–1641, 2009.

A. Warrick, J.W. Biggar, and D.R. Nielsen. Simultaneous solute and water transfer for an unsaturated soil. *Water Resour. Res.*, 7(5):1216–1225, 1971.

N. Watanabe. *Finite element method for coupled Thermo-Hydro-Mechanical processes in discretely fractured and non-fractured porous media*. PhD thesis, TU Dresden, 2012.

S. Whitaker. The equations of motion in porous media. *Chem. Eng. Sci.*, 21(3):291300, 1966.

S. Whitaker. Advances in theory of fluid motion in porous media. *Ind. Eng. Chem.*, 61(12): 1428, 1969.

G.T. Yeh. On the computation of darcian velocity and mass balance in the finite-element modeling of groundwater-flow. *Water Resour. Res.*, 17(5):1529–1534, 1981.

Y. Zhang, D.A. Benson, M.M. Meerschaert, and E.M. LaBolle. Random walk approximation of fractional-order multiscaling anomalous diffusion. *Physical Rewiew*, E 74 (026706):10pp, 2006.